INFORMATION TO USERS

This manuscript has been reproduced from the microfilm master. UMI films the text directly from the original or copy submitted. Thus, some thesis and dissertation copies are in typewriter face, while others may be from any type of computer printer.

The quality of this reproduction is dependent upon the quality of the copy submitted. Broken or indistinct print, colored or poor quality illustrations and photographs, print bleedthrough, substandard margins, and improper alignment can adversely affect reproduction.

In the unlikely event that the author did not send UMI a complete manuscript and there are missing pages, these will be noted. Also, if unauthorized copyright material had to be removed, a note will indicate the deletion.

Oversize materials (e.g., maps, drawings, charts) are reproduced by sectioning the original, beginning at the upper left-hand corner and continuing from left to right in equal sections with small overlaps. Each original is also photographed in one exposure and is included in reduced form at the back of the book.

Photographs included in the original manuscript have been reproduced xerographically in this copy. Higher quality 6" x 9" black and white photographic prints are available for any photographs or illustrations appearing in this copy for an additional charge. Contact UMI directly to order.

UMI

A Bell & Howell Information Company
300 North Zeeb Road, Ann Arbor MI 48106-1346 USA
313/761-4700 800/521-0600

AN INVESTIGATION OF POWDER GRANULATION BY EXPERIMENTS AND NUMERICAL SIMULATION

by

M. IRFAN KHAN

A dissertation submitted to the Graduate Faculty in Engineering
in partial fulfillment of the requirements for the degree of Doctor of Philosophy.
The City University of New York

1998

This manuscript has been read and accepted for the Graduate Faculty in Engineering in satisfaction of the dissertation requirement for the degree of Doctor of Philosophy.

September 1994 — Date

Chair of Examining Committee

September 16, 1994 — Date

Executive Officer

Gabriel I. Tardos (Mentor)

Robert A. Graff

Leslie L. Issacs

Herbert Weinstein

Stelios C. Tsinontides

Supervisory Committee

The City University of New York

Abstract

AN INVESTIGATION OF POWDER GRANULATION
BY EXPERIMENTS AND NUMERICAL SIMULATION

by

M. IRFAN KHAN

Advisor: Professor Gabriel I. Tardos

The objective of present work is to develop a model of granulation process, which predicts product properties of from a knowledge of operating conditions. Granulation is essentially a solid-particle agglomeration process. It improves bulk powder properties like density, flowability, solubility etc., and is an extensively used unit operation in chemical, mineral, pharmaceutical and food industries. Our primary aim in this work is to understand the micro-level physics of this process, and arrive at a macro-level model which relies on a minimal number of readily estimable parameters.

We begin in Chapter 1 by reviewing some basic concepts in granulation modelling. We then proceed to develop a simple model which predicts the mean size of agglomerated product. This model attempts to incorporate the influence of important, and also to a large extent hitherto unexplored, effects of agglomerate breakup. Furthermore, we identify the important problem of deformation and breakup of agglomerates in a shearing medium, and analyze this in Chapter 2. There we also develop two new tools of analysis: those of experiments using a fluidized-bed granular-flow Couette device, and a computer simulation of shear flows of solid particles.

The experimental setup is useful in creating an environment in which particles can flow under conditions of approximately constant, and known, shear. We use this experimental setup to analyze the problem of deformation and breakup of wet agglomerates in a shearing medium. Study of this problem provided useful insight into

the micro-level agglomerate breakup phenomenon at work during granulation. Subsequently, we also demonstrate the usefulness of this device in carrying out rheometric studies on flowing solid particulate systems.

The computer simulation serves as a good tool of integrating the micro-level forces and providing an accurate macro-level description of solid-particle flow processes. The central philosophy behind the simulation is to model inter-particle interactions, and compute the individual particle trajectories which result from these interactions. We apply this tool to analyze the problem of shear induced deformation and breakup of wet agglomerates, and compare the results with those obtained from experiments.

In Chapter 3 we improve upon the simulation developed in Chapter 2 by directly simulating an idealized wet granulation experiment. In this model we essentially simulate a shear flow of a system of solid particles, some of which are wet, while the rest dry. This simulation model provides for a complete model of granulation process, in which the properties of the agglomerates like their size, shape and density can be inferred from the input parameters of the simulation. Due to the limitations of the present model we are able to relate these properties only in a qualitative sense. An accurate quantitative relation between these input and output properties can be achieved by means of some further work on the simulation model. Practical means of incorporating these improvements are also discussed.

Acknowledgments

I would like to thank my advisor, Professor Gabriel Tardos, for his help with this work. He has been a continued source of good ideas, many of which I was able to successfully implement in this work. I would also like to thank the faculty of the Chemical Engineering department. Things that I have gained from them during course-work and personal interaction, define in many respects my present professional capabilities. I thank the very talented technicians of our department, Zhen Rong Xu, Ivan Ortiz and Andrew Eng. They have helped in accomplishing the quite difficult job of building the experimental setup of this work. Andrew Eng in addition has endured with my endless 'computer-problems'.

My thanks are also due to Dr. Badraddine Ahtchi-Ali of Unilever Research U.S., for providing me with an opportunity to spend a semester at Unilever Research. This has enabled me to experience some 'real-world' issues in Powder Technology, while at the same time has given me an opportunity to interact with people and experience the work environment at Unilever Research. I thank Professor Michael Louge of Cornell University for taking interest in my work, and for helpful advice. I also thank Dr. Stelios Tsinontides of Merck Research Laboratories for being a member of my doctoral committee, and for fruitful discussions.

Finally, I acknowledge the support in the form of computer time provided by the National Center for Supercomputing Applications, University of Illinois at Urbana Champaign. They have provided access to a state-of-the-art computing environment, and also to a very helpful and knowledgable staff. This has greatly enhanced my ability to carry out simulations during this work.

Contents

List of Tables

List of Figures

Chapter 1

Preliminary concepts and a basic model

1.1 Particle agglomeration processes and their terminology

A particulate material in which the individual particles are agglomerates made up of still finer particles, is referred to as being agglomerated. Agglomeration is useful for improving bulk particle properties like density, flowability, dispensability etc. and to reduce dustiness. For a mixture of different powder types, such as in many pharmaceutical formulations, agglomeration provides resistance against component segregation and is therefore usually a prerequisite for tablet compression. Many powdery food products are agglomerated in order to have pleasant appearance and good 'instant' properties such as wettability, sinkability, dispersibility and solubility.

Agglomeration is carried out by agitating the powder mass in the presence of a 'binding-agent', usually a polymeric substance, which serves to bind the individual particles together in the agglomerates. If the binding agent used during the agglomeration process is in a liquid solution form, the process is called wet agglomeration, while if it is a molten liquid which solidifies at ambient temperature, it is called a

melt agglomeration process. An agglomeration process that results in somewhat non-spherical agglomerates with a rather wide size distribution within the range of about 0.1 to 2 mm is named a *granulation* process and the agglomerates are called granules. If the final agglomerates are somewhat spherical and of a narrow size distribution in the size range of about 0.5 to 2 mm. the process is called *pelletization* and the agglomerates are called pellets (Schaefer (1997)). The present work concerns **wet granulation** processes.

1.2 Wet granulation processes and equipment

Agglomeration in wet granulation is carried out by spraying onto an agitating powder mass, a controlled amount of binder liquid to yield wet agglomerates. Movement in the powder mass is induced by an apparatus such as a rotating drum, fluidized bed or a high-shear mixer. Local conditions of shear in the moving powder mass serve to induce both coalescence as well as breakage of wet agglomerates and hence define a steady agglomerate size. Wet agglomerates are subsequently dried to yield the final product in which particles are bound together by solid bridges left behind by the binder fluid. Several commercial designs of wet granulation equipment (called granulators) are popular. The basic requirement among various design alternatives is to provide a shear environment to the powder being granulated while also providing a facility for the addition of binding agent. Following are a few popular ones:

Rotary-Drum granulator: It is a hollow cylindrical drum, partially filled with particles, in which rotation of the drum provides shear to the particles. The axis of rotation may be horizontal or inclined at a slight angle to the horizontal. Particles are lifted along the walls either by friction or by vanes attached to the walls and fall down from a height which can be controlled by the rate of rotation. Binder is usually sprayed on to the falling curtain of particles. The magnitude of shear imparted to

the powder in this design is low.

Fluid-Bed granulator: As the name suggests, particles in this granulator are contained inside a fluidized bed. The flow behavior of particles inside the bed, governed by the fluidizing air flow and the nature of particles, governs the amount of shear. Binder is usually sprayed from the top of the bed. The magnitude of shear obtained in this kind of equipment can vary from low (in a bed operating near minimum bubbling conditions) to moderately high (in a vigorously bubbling bed). An additional advantage of the Fluid-Bed granulator is that the agglomerates can be dried, and if a subsequent coating with a different substance is desired, can also be coated in the same apparatus.

High-Shear Mixer granulator: Particles here are contained inside a pan-like vessel which is equipped with a rotating impeller to impart shear forces. The arrangement is similar to the mixing devices used for mixing fluids. The binder is introduced at the top of the powder bed. The magnitude of shear obtained with this kind of device is quite high. The quality of agglomeration achieved with this apparatus is good, but the large shear forces also lead to large generation of heat in the powder mass and hence this apparatus cannot be used to granulate powders which are sensitive to, and/or degrade with, heat.

A commercial granulator can also be a hybrid of the above mentioned types such as the one in which a rotating impeller is present in a bed of fluidized particles (Watano et al. (1997)). In other designs an impeller blade is present inside a rotating drum, while in yet others, particles in a rotating drum are kept in a fluidized state. The design may also be of an entirely different kind such as the "Jet granulator" (Hogekamp et al. (1996)) in which there are no mechanical parts and an air jet

imparts shear forces to the particles.

1.3 Past wet granulation modelling

Early attempts at modelling granulation process were based on population balance techniques, and followed an approach similar to that taken in modelling coagulation of aerosols (Ramabhadran (1975)). The central element in this modelling technique is the population balance equation, which is a generalized differential balance equation over time and spatial coordinates of particle properties such as their size (Hulburt and Katz (1964)). This equation can be applied in general to model any process involving change in particle properties with respect to some coordinates, and its solution in principle provides a complete description of the process. In practice, however, this proves to be difficult because the equation involves some unknown functions of the coordinates and the particle properties (the birth and death functions, which in the case of granulation are the growth and breakage functions). The form of these functions is not provided by the theory, instead their nature depends upon the phenomenon at micro-level (in granulation, the physics of agglomerate coalescence and breakage). Apart from some very simple and idealized process, the nature of these unknown functions can at best be guessed from a regression analysis of the experimental data. Though still a very powerful and versatile one, the technique would classify more as a regression technique rather than one which arises from a fundamental investigation of the process. In the present work we have not considered modelling based on population balance techniques.

A model that focused on the fundamental physics of granulation process was proposed first by Ennis et al. (1991). The model evolved out of the research in agglomeration in high temperature fluidized beds (Compo (1989)), and rests on an evaluation of the conditions required for a successful coalescence of two wet, colliding agglomerates. The tendency towards coalescence was estimated by the magnitude of a dimensionless parameter called the Stokes number, St. This represents the ratio of

the relative kinetic energy of approach between two colliding agglomerates which are wet on their outer surface, to the viscous dissipation occurring in the liquid bridge formed between them, and was defined as:

$$St = \frac{4\rho_a U_{rel} d_a}{9\mu} \tag{1.1}$$

where ρ_a is the density of the colliding agglomerates, U_{rel} is the relative velocity of approach between them, d_a is the diameter of the colliding agglomerates and μ if the viscosity of the liquid binder which wets the surface of the constituent particles. At low values of St, the colliding agglomerates tend to coalesce and at high values of St they tend to rebound at their outer surface. The value of St at which these two tendencies are exactly balanced was termed as the critical Stokes number, St^*. This critical number was shown to be a constant parameter for a given system, and was also evaluated analytically as: $St^* = (1 + 1/e)\ln(h/h_a)$, where e is the coefficient of restitution of the constituent particles, h is an estimate of the thickness of the wet layer over the surface of particles, and h_a is a measure of the magnitude of the asperities present on the surface of particles.

According to the above analysis, the steady state size of agglomerates in a given granulating system can be estimated by equating the Stokes number of the system to its critical value. The model was supported by fluidized bed granulation experiments of Ennis et al. (1991). Subsequently it has also been found suitable for a qualitative description of an agglomeration process in a drum granulator as well as in a high-shear mixer (Schaefer (1997)). At the same time the approach has been criticized because of its overly simplistic view of the nature of process. A main drawback is that the model views the colliding agglomerates as rigid, non-deformable entities, and property changes only due to coalescence are considered while an equally important phenomenon of agglomerate breakup is glossed over. Agglomerate breakup is now regarded to be one of the main phenomenon influencing the steady state properties

of the agglomerates (Simons (1996)). It has not been widely researched because by its very nature it is also quite an unpredictable phenomenon, not easily analyzed by conventional analytical tools. In the next section we develop a simple model of the wet granulation process, which puts the above model in perspective while at the same time also attempts to incorporate the effect of agglomerate breakup.

1.4 A model incorporating agglomerate breakup

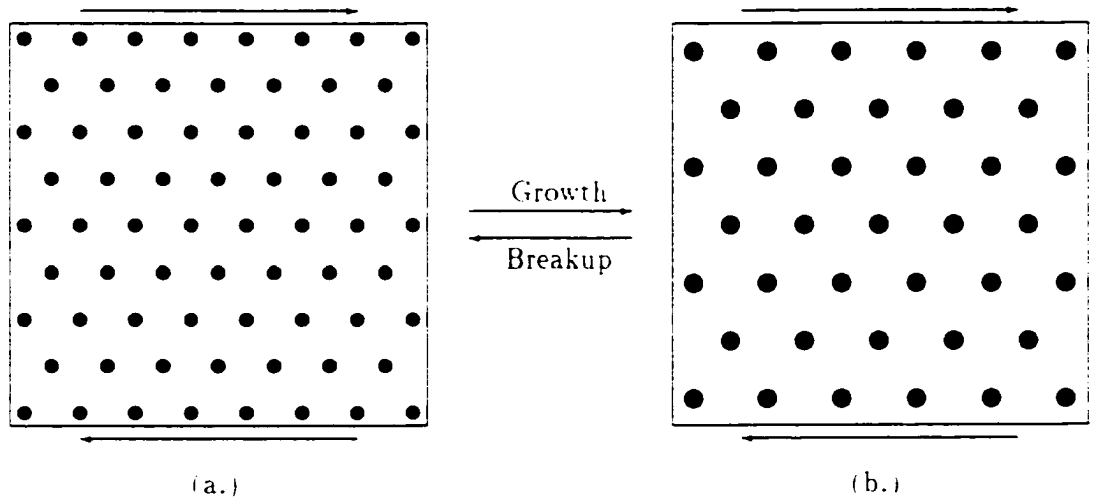

Figure 1.1: An idealized wet granulation experiment in which identical conditions throughout the domain lead to a constant agglomerate size. At equilibrium, this size is determined by relative magnitudes of the growth and breakup forces.

Consider wet granulation in a uniform shear environment of a monodisperse powder of a constant initial particle size d_p. Further assume these particles to be spherical and coated on their outer surface with a binder layer of constant thickness h. In this environment the powder would undergo first an agglomeration of individual particles, forming doublets, triplets etc., and subsequently a further growth in agglomerate size due to inter-agglomerate coalescence. As the agglomerates grow, at some point the

system would also start exhibiting agglomerate breakup due to an increase in inertial forces resulting from the increased size of the shearing agglomerates. The relative magnitude of these two forces (coalescence versus breakup), would determine the final equilibrium agglomerate size. The situation is depicted schematically in Figure 1.1. Since the individual particles are identical, having identical surface-wetting characteristics, and being exposed to identical conditions of shear, the resulting agglomerates would also be identical because of the identical conditions prevailing during their formation, growth and breakup. We hence assume that the resulting agglomerates at equilibrium carry identical properties like size, shape and density. These steady state properties are a function only of the relative magnitude of growth and breakup forces. In order to quantify the nature of these forces, we identify three main kinds of energies associated with the shearing agglomerates in the present system:

1. Kinetic energy possessed by the shearing agglomerates, E_k.

2. Energy dissipation required in the wet layer for two colliding agglomerates to coalesce, E_c.

3. Energy required to deform and break the agglomerates by shearing them at the prevailing shear rate, E_s.

Under the assumption that these energies act independently, some estimates can be made about their nature. For an estimate of E_k, we identify the properties that characterize the kinetic energy of flowing agglomerates. These are the agglomerate diameter d_a, the agglomerate density ρ_a, and the shear rate $\dot{\gamma}$. The only combination of these quantities that could yield an energy term is $\rho_a \dot{\gamma}^2 d_a^5$, thus leading to a following form for E_k:

$$E_k = C_1 \rho_a \dot{\gamma}^2 d_a^5 \tag{1.2}$$

where C_1 is a dimensionless constant. For an estimate of E_c, consider the dissipation

that occurs when two surface-wet particles collide. Ennis et al. (1991) present an approximate solution for this dissipation for a given relative velocity of approach between two particles before collision, U_{rel}. A characteristic value of U_{rel} in the present system is $\dot{\gamma} d_a$. The following form for E_c then follows from their analysis:

$$E_c = C_2 \mu \dot{\gamma} d_a^3 \tag{1.3}$$

where C_2 is a dimensionless constant. The above expression is based on the assumption that the dissipation occurring in the wet layer is entirely viscous in nature and that surface tension effects play a negligible role. This is proven by Ennis et al. (1990) to be a justified assumption under most practical conditions. For an estimate of E_k, consider the rate of energy input required to make the agglomerate flow at a shear rate of $\dot{\gamma}$. This rate of energy per unit volume is proportional to $\tau(\dot{\gamma})\dot{\gamma}$ (stress times strain), where $\tau(\dot{\gamma})$ represents the shear-stress response of the agglomerate. The energy required to make the agglomerates flow at shear rates of $\dot{\gamma}$ for times scales of $\dot{\gamma}^{-1}$ is thus proportional to $\tau(\dot{\gamma}) d_a^3$. We assume that the agglomerate will break if it deforms an 'appreciable' rate over time scales which are typical in the present system. The time scales in the present system are of the order $\dot{\gamma}^{-1}$. An 'appreciable' rate of deformation is thus also considered as one which occurs as a result of flow with a shear rate of $\dot{\gamma}$. This leads to a following form for the energy required to deform and break the agglomerate:

$$E_b = C_3 \tau(\dot{\gamma}) d_a^3 \tag{1.4}$$

where C_3 is a dimensionless constant.

The ratio E_k/E_c gives an estimate of the magnitude of growth forces. Values of this ratio of less than 1 imply that the agglomerate tend to coalesce after a collision and grow whereas values of greater than 1 imply that they tend to bounce back at

their surface after a collision and stop growing. Similarly the ratio E_k/E_b gives an estimate of the magnitude of the breakup forces. Values of this ratio of less then 1 imply that the agglomerates survive breakage due to shearing forces, while values greater than 1 imply that the shearing forces result in their breakage. These two ratios, E_k/E_c and E_k/E_b, can be written from the above equations as:

$$\frac{E_k}{E_c} = \frac{\frac{\rho_a \dot{\gamma}^2 d_a^2}{\mu}}{\frac{C_2}{C_1}} = \frac{St}{St_c^*} \tag{1.5}$$

$$\frac{E_k}{E_b} = \frac{\frac{\rho_a \dot{\gamma}^2 d_a^2}{\mu(1-\varepsilon)}}{\frac{C_3}{C_1}} = \frac{St_b}{St_b^*} \tag{1.6}$$

The numerator in the expression for E_k/E_c represents the ratio of inertial forces in the flow to the dissipative ones in the wet layer, and is termed as the coalescence Stokes number, St. The numerator in the expression for E_k/E_b represents the ratio of inertial forces in the flow inducing the breakage of agglomerates to the ones resisting it, and is termed as the breakage Stokes number, St_b. The ratios C_2/C_1 and C_3/C_1 are dimensionless numbers which depend upon system properties like the solid fraction and the binder relative saturation (which determines the wetting layer thickness), and which are assumed to be constants for a given system. The value of St when E_k and E_c exactly balance each other is denoted by St_c^* (the critical Stokes number for agglomerate coalescence), and hence St_c^* is equal to C_2/C_1. Similarly the value of St_b when E_k and E_b exactly balance each other is denoted by St_b^* (the critical Stokes number for agglomerate breakage), and hence it is equal to C_3/C_1. For a given granulation system operating under conditions of constant shear, the dependence of the ratios E_k/E_c and E_k/E_b on the size of agglomerates d_a as obtained from the above equations is shown in Figures 1.2 and 1.3. Figure 1.2 considers the case when the curve for E_k/E_c lies above the one for E_k/E_b and Figure 1.3 considers the case when it lies below.

Consider what happens in Figures 1.2 and 1.3 as we start granulating a powder,

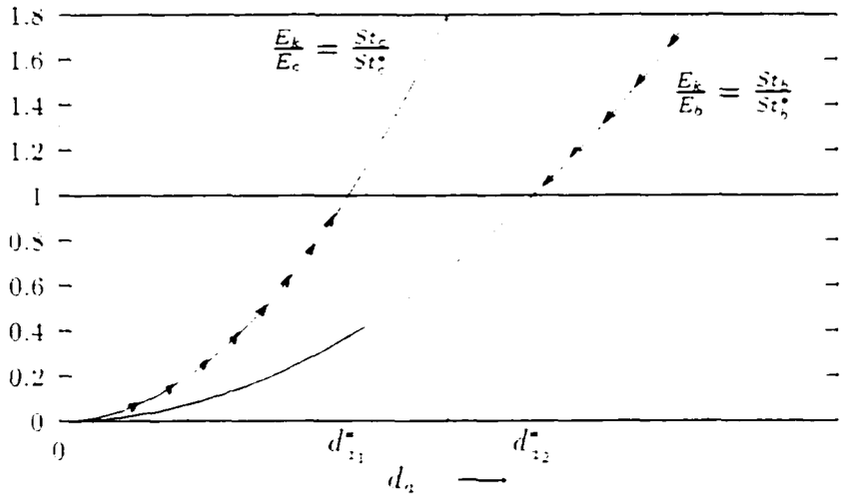

Figure 1.2: The dependence of E_k/E_c and E_k/E_b on d_a for the case when $E_k/E_c > E_k/E_b$. Arrows on the curve represent a drift from an unstable operation to a stable one.

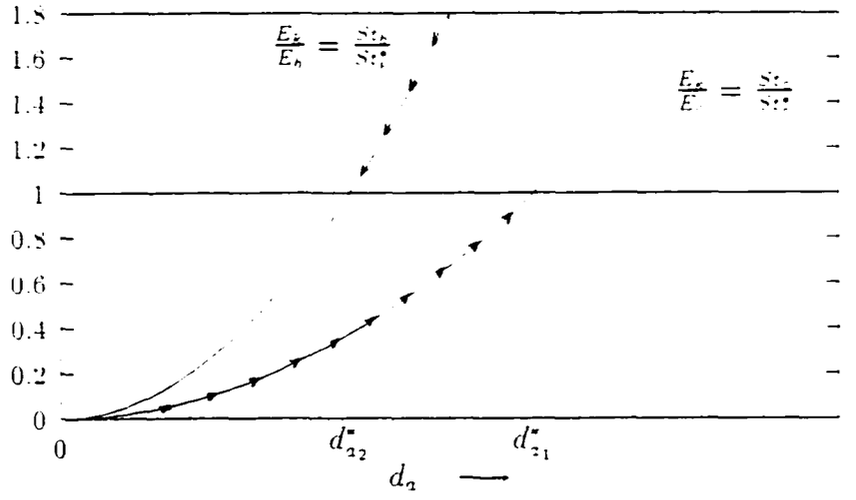

Figure 1.3: The dependence of E_k/E_c and E_k/E_b on d_a for the case when $E_k/E_c < E_k/E_b$. Arrows on the curve represent a drift from an unstable operation to a stable one.

progressing from a very low value of d_a (close to d_p) to a higher one. At low values of d_a, $E_k/E_c < 1$. In other words, kinetic energy supplied to the agglomerates by the flow is less than what can be dissipated during a collision. Hence they coalesce and result in a higher value of d_a. The process continues until $E_k \geq E_c$, when tendencies towards further growth disappear. If some agglomerates grow to an extent such that they find themselves in a region where $E_k/E_b > 1$, they break apart resulting in a lower value of d_a. It is these competing effects of growth and breaking that make the system drift towards a steady state value of d_a. The part of the curve where a value of d_a is unstable is marked by arrows. The direction of arrows represent the direction of drift towards a stable operation. If d_a increases very gradually from the start of the operation, the system will find a steady state in Figure 1.2 at $d_{a_1}^*$ and in Figure 1.3 at $d_{a_2}^*$. If the progression is not very gradual however, one would expect a spread in sizes towards $d_{a_2}^*$ in the first case and towards $d_{a_1}^*$ in the other.

Another conclusion that can be drawn from the above analysis is that if the granulating system operates at conditions where the size is mainly determined by a limitation on coalescence, as in Figure 1.2, the steady state agglomerate size, d_a^*, can be found by equating St_c to St_c^*, and when the size is mainly determined by a limitation on breakage, as in Figure 1.3, d_a^* can be found by equating St_b to St_b^*. Since St_c^* and St_b^* are constants for a given powder-binder system, the above can be expressed as:

For granulation occurring under a coalescence limitation:

$$St_c = \frac{\rho_a \dot{\gamma} d_a^{*2}}{\mu} = \text{Constant} \tag{1.7}$$

and for granulation occurring under a breakage limitation:

$$St_b = \frac{\rho_a \dot{\gamma}^2 d_a^{*2}}{\tau(\dot{\gamma})} = \text{Constant}. \tag{1.8}$$

A constitutive relation for $\tau(\dot{\gamma})$, relating it to $\dot{\gamma}$, is needed in order to find the dependence of St_b on $\dot{\gamma}$. The agglomerates are essentially concentrated suspensions

of particles in the binder fluid. Under most practical situations, such suspensions follow a general Herschel-Bulkley type flow model (Adams et al. (1993)):

$$\tau(\dot{\gamma}) = \tau_y + k\dot{\gamma}^n \tag{1.9}$$

where τ_y is the yield stress, k is the shear flow consistency and n is known as the shear flow index. Contribution of the yield stress usually becomes important when the particle size approaches the colloidal limit (about 1 μm), the particle volume fraction approaches the maximum limit, or as the shear rate approaches zero (Turian et al. (1992)). In the present discussion we assume that none of the above requirements are met, so that the contribution of the yield stress in the Herschel-Bulkley model can be neglected. The stress $\tau(\dot{\gamma})$ under these conditions becomes $k\dot{\gamma}^n$. Under the assumption of uniform agglomerate properties (like their density), k can be taken as a constant. Hence for granulating systems operating under identical conditions except for the imposed shear rate, equations 1.7 and 1.8 imply that $\dot{\gamma}\, d_a^2 = \text{Constant}$ for granulation occurring under a coalescence limitation, and $\dot{\gamma}^{(2-n)} d_a^2 = \text{Constant}$ for granulation occurring under a breakage limitation. These two expressions can be rewritten as:

For granulation occurring under a coalescence limitation:

$$\log(d_a) = -\frac{1}{2}\log(\dot{\gamma}) - \text{Constant} \tag{1.10}$$

and for granulation occurring under a breakage limitation:

$$\log(d_a) = -\left(1 - \frac{n}{2}\right)\log(\dot{\gamma}) + \text{Constant} \tag{1.11}$$

A logarithmic plot of d_a versus $\dot{\gamma}$ hence predicts a straight line of slope $-(1/2)$ for a coalescence limited granulation and a slope of $-(1 - n/2)$ for a breakage limited granulation.

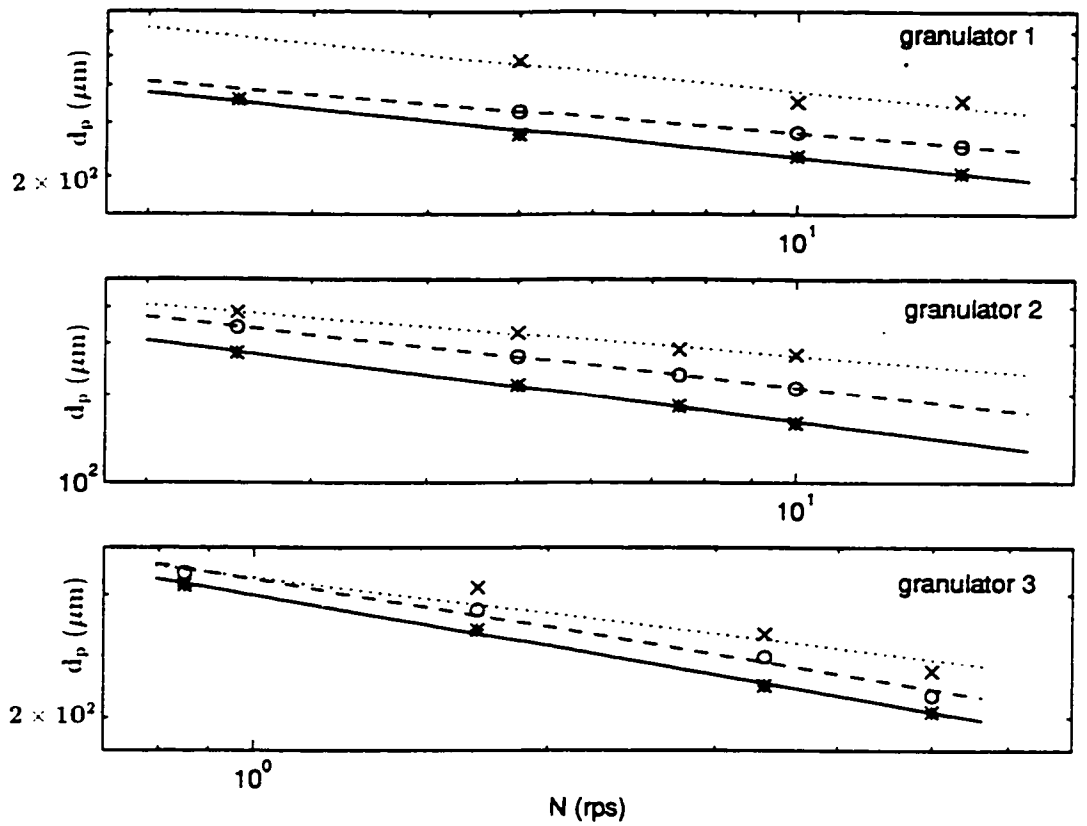

Figure 1.4: A log-log plot of d_a (μm) versus the impeller rotation speed N (rev./sec.) for the experimental data of Watano et al. (1997) for three different types of fluid-bed high-shear mixer type granulators. The symbols '*', 'o' and 'x' represent the three different data sets, each of which was obtained by changing N only.

In order to test the above analysis, data of Watano et al. (1997) is compared to the prediction of the model. These authors have carried out granulations of a pharmaceutical standard formulation (average $d_p = 45$ μm) in fluid-bed high-shear mixer type granulators of three different dimensions. For each granulator, their experimental results contain sets of data points for agglomerate sizes d_a obtained for different impeller rotation speeds N, rest of the conditions being identical for a particular set. For a given granulator, N should be proportional to the imposed shear rate $\dot{\gamma}$, hence replacing $\dot{\gamma}$ by N in equations 1.10 and 1.11 should affect only the constant term and a log-log representation of d_a versus N for a particular data set should result in a straight line. Figure 1.4, which is a log-log representation of their set of data points of d_a versus N, supports this conclusion. A data set is fitted to an equation of the type $\log(d_a) = m \log(N) + c$ where d_a is measured in μm and N in revolutions per sec. Table 1.1 gives the values of m and c obtained for different data sets.

Table 1.1: Values of m and c obtained by fitting the data sets in Figure 1.4 to the equation $\log(d_a) = m \log(N) + c$

Data Set	Granulator 1		Granulator 2		Granulator 3	
	m	c	m	c	m	c
1 ('*')	−0.30	2.67	−0.39	2.60	−0.23	2.47
2 ('o')	−0.24	2.68	−0.34	2.67	−0.22	2.49
3 ('x')	−0.30	2.88	−0.25	2.68	−0.16	2.50

The values of m in Table 1.1 when compared with the expressions for slope in Equations 1.10 and 1.11 indicate that the granulation belongs to the breakage limited case. An average value of m obtained from Table 1.1 is −0.27. This gives a value of the shear flow index n from Equation 1.11 as 1.46, which indicates that the agglomerates behave as shear thickening. Concentrated suspensions of particles may behave in this fashion (Macosko (1993)), and the value of n can also be in this range. An important conclusion is that both the slope, m, and the coefficient, c, take approximately the

same value for granulators of different size operated under different conditions. This indicates that the above analysis is well suited not only for characterizing a given granulation system but also for a scale-up of the underlying equipment.

So far we have been able to demonstrate the validity of our proposed model by comparing it to an experimental data set. In order to use it as a self consistent model of granulation we would need to find the dependence of St_c^* on system properties. It was noted earlier that St_c^* depends upon constant system properties such as the solid fraction and binder relative saturation, and that the dependence of St_c^* on them arises from the physics of deformation and breakup of individual agglomerates. In an attempt to evaluate this dependence, we analyze in next chapter the phenomenon of shear induced deformation and breakup of wet agglomerates.

Chapter 2

Stability of wet agglomerates in a shearing medium

As was noted in the previous chapter, the model of wet granulation that we developed can be made complete and self consistent if one can relate the deformation and breakup characteristics of individual agglomerates to a parameter such as the breakage Stokes number, St_c. The deformation and breakage of agglomerates in this model results from their interaction with the surrounding, identical shearing wet agglomerates. This system is somewhat difficult to study in practice because an agglomerate is part of a system containing numerous objects which are identical to it, and also because it is present in a dynamic environment in which a rapid coalescence and fragmentation of these entities is occurring. Due to these reasons it becomes difficult to study the behavior of an individual agglomerate in isolation. The difficulties can be overcome to a large extent however in a somewhat related setting, in which an individual agglomerate is surrounded not by other identical wet agglomerates, but by a dry granular material. An agglomerate can then be easily identified as a separate entity until its point of breakup into smaller pieces, while an added advantage is that the flow of surrounding granular material is also much easier to control. This chapter is devoted to a careful study of this problem. We begin by first formulating the

problem and identifying the dimensionless parameters. Subsequently we present the analysis by means of computer simulations and experiments.

2.1 Problem formulation

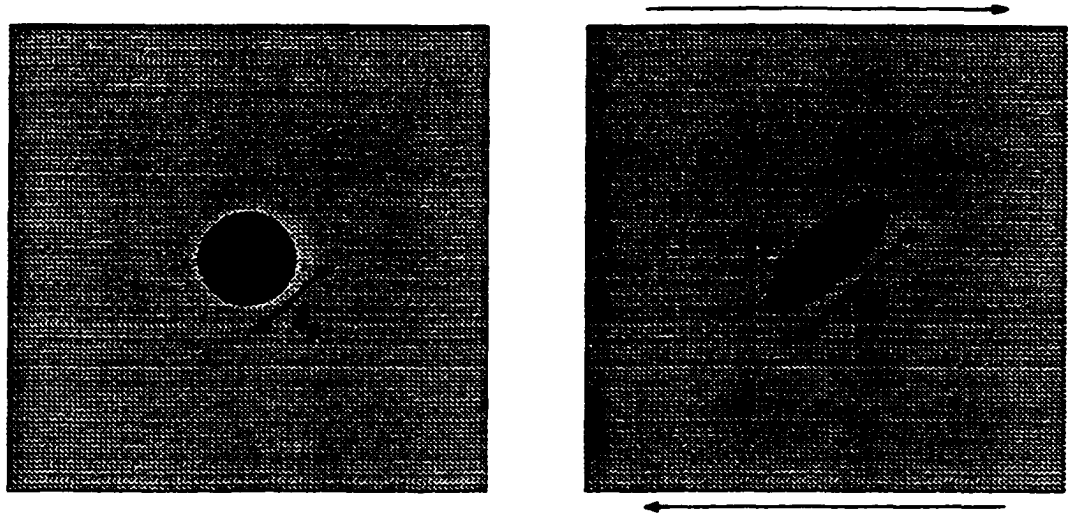

Figure 2.1: A wet agglomerate in a granular medium which is (a.) stationary and (b.) sheared. The spherical wet agglomerate in part (a.) deforms by stretching in part (b.).

The problem that we seek to analyze is depicted schematically in Figure 2.1. An initially spherical wet agglomerate in a stationary granular medium (Figure 2.1(a.)), starts deforming by stretching when the surrounding granular medium is sheared (Figure 2.1(b.)). This behavior has been observed during experiments (see section 2.4), where a shear field of granular solids is created in a fluidized bed Couette device, and the response of wet agglomerates in this shearing granular medium is studied. Experimental results indicate that if the degree of deformation exceeds a particular limit, wet agglomerates become susceptible to breakage. The degree of deformation depends on system parameters such as the properties of the wet agglomerate, those of the granular medium and upon the imposed shear rate. In this chapter we aim to evaluate this dependence by means of a computer simulation model, and subsequently compare the results with those obtained from experiments.

The force inducing deformation of the agglomerate in Figure 2.1 is the inertial force due to the surrounding granular medium. The force resisting its deformation is the viscous drag opposing the movement of individual particles in it. The ratio of these two forces (inducing to resisting) can be expected to govern the dynamics of deformation of the agglomerate. Tendency towards deformation (and hence breakage) should be large for large values of this ratio and vice versa. The ratio of particle inertia to the viscous drag has been referred to in the literature as the Stokes number (Koch (1990)). We have hence termed the present ratio as the deformation Stokes number, St_{def}, which can be written as:

$$St_{def} = \frac{\rho_{p_g} U_g^2}{\mu U_a / d_{p_a}} \tag{2.1}$$

The numerator in the above expression represents the characteristic inertial force in the surrounding granular medium, where ρ_{p_g} and U_g are particle density and its characteristic velocity, respectively. The denominator represents the characteristic viscous force in the agglomerate, induced as a result of a particle moving relative to the interstitial fluid with a characteristic velocity U_a in the Stokes flow regime, where μ is the viscosity of the interstitial fluid and d_{p_a} is the diameter of a particle within the agglomerate phase. If $\dot{\gamma}$ is the imposed shear rate, a characteristic particle velocity in the agglomerate phase is $d_{p_a}\dot{\gamma}$, while that in the granular phase is $d_{p_g}\dot{\gamma}$, where d_{p_g} is the diameter of a particle within the granular phase. The expression for St_{def} then simplifies to:

$$St_{def} = \frac{\rho_{p_g} d_{p_g}^2 \dot{\gamma}}{\mu} \tag{2.2}$$

As a measure of the degree of deformation (by elongation) of the agglomerate, we introduce the Elongation parameter, E, defined as:

$$E = \frac{l}{d_o} \tag{2.3}$$

where d_o is the diameter of the original undeformed (spherical) agglomerate and l the major axis of the deformed one (Figure 2.1). The range of experimentally observed values of E lies between 1 (for zero deformation) and 1.5 (for highly deformed agglomerates). E can be used as a measure of the agglomerate's tendency towards breakage. Low values of E would imply a low tendency towards breakage and vice versa. The objective of analyzing the present problem then reduces to correlating E with St_{def}.

The deformation Stokes number, St_{def}, defined above is different from the breakage Stokes number, St_b, introduced in the previous chapter. Both numbers represent the ratio of forces inducing the deformation and breakup of agglomerates (inertial forces) to the ones resisting it (the viscous forces). They however represent this ratio in two different settings. The deformation Stokes number, St_{def}, represents this ratio for a case where an individual agglomerate is surrounded by shearing dry particles, while the breakage Stokes number, St_b, represents it for a case when the surrounding medium is composed of identical shearing wet agglomerates. The manner in which viscous resistance is captured in the two numbers is also different. Viscous forces in St_{def} represent the resistance offered to the movement of individual particles in the agglomerate and assume a Newtonian type flow behavior, while in St_b they represent the resistance offered to the deformation of agglomerate as a whole and assume a power-law type flow behavior.

2.2 The computer simulation model

A computer simulation model is developed to analyze the above problem. The model is based on the discrete element approach for simulating flows of a granular material, and of a suspension of particles. The two approaches, applied separately in the gran-

ular or the external phase, and the agglomerate or the interior phase, are discussed further in the following two subsections.

2.2.1 Granular phase

Particles in the granular phase are modeled as smooth rigid spheres of uniform size. The interstitial fluid is assumed to be of very low density and viscosity (such as air), so that it plays no significant part in momentum transfer. Particle trajectories between successive collisions can then be approximated by Newton's equation of motion. A computer simulation of the flow of such particles computes trajectories between two successive collisions and modifies them appropriately during a collision by satisfying the conservations of linear/angular momentum and energy. The inter-particle interactions during a collision are usually characterized by two parameters: the coefficient of restitution, ϵ (the ratio of approach to recoil velocities), and the coefficient of surface friction, σ. Both these parameters are usually taken as constant particle properties. In the present simulations the only parameter of interest is (ϵ), since the particles are considered to be smooth on their outer surface.

There are several such simulations in literature. Existing simulation techniques mainly differ from one another in the manner they satisfy the conservation of linear/angular momentum and energy during a collision, and upon the definition of conditions under which a collision is assumed to occur. These techniques can be broadly classified into three main types (Hopkins & Louge (1990)): hard-particle collision, soft-particle contact and hard-particle overlap models. The hard-particle collision model assumes the particles to be hard spheres and hence a collision is assumed to occur instantly upon contact. During a collision the colliding particle pair undergoes an instantaneous change in its linear/angular momentum, the change being a function of the coefficients of restitution and surface friction. The model progresses in time by searching for the most imminent collision in the system (the closest point in time at which any two particles in the system just touch), moving the system to the point

of this collision, and then executing the collision. In soft-particle contact model the particles are modeled as deformable on their outer surface. The simulation proceeds by moving the system ahead over small predetermined time intervals after which the particles overlap slightly. The overlaps are interpreted as deformations and a repulsive force based on a spring and dashpot model is generated. The properties of this model are chosen such that the collision outcome is consistent with the chosen values of ϵ and σ. The hard-particle overlap model combines the above two approaches by modeling particles as rigid spheres while also allowing for an overlap. The simulation proceeds over small time intervals, after each one of which the overlaps between particles are checked and a collision is executed whenever one is detected. The time interval is kept low enough so that on an average only a very tiny fraction (say 1%) of the particle diameter is overlapped and the system properties such as the stresses in flow become independent of a further reduction in the time interval. Each model is suitable for simulating flows in a particular density range: hard-particle collision model in the low density, soft-particle contact in the high density and hard-particle overlap model in the intermediate density range. In the current problem we deal with flows in the intermediate density range and hence we have used the hard-particle overlap model, developed by Hopkins & Louge (1990), in the present simulations.

For computational efficiency we have simulated the flow of spheres, the motion of which are restricted to lie in a plane. While an idealization, this type of flow has been regarded as a good approximation for three-dimensional shear flows of granular materials as well as that of suspensions, since the pair distribution functions in the two cases are expected not to differ significantly from one another (Bossis and Brady (1984)). Experiments with such systems, involving granular materials (Aidanpää et al. (1996)) as well as suspensions (Bouillot et al. (1982)), have also been performed. This shows that these type of flows are also practically realizable. The simulation domain along the plane of particle movement is rectangular with horizontal and vertical edge dimensions equal to L_x and L_y respectively. The domain is surrounded on all four sides by mirror images as is shown in Figure 2.2. If image boxes at the top are

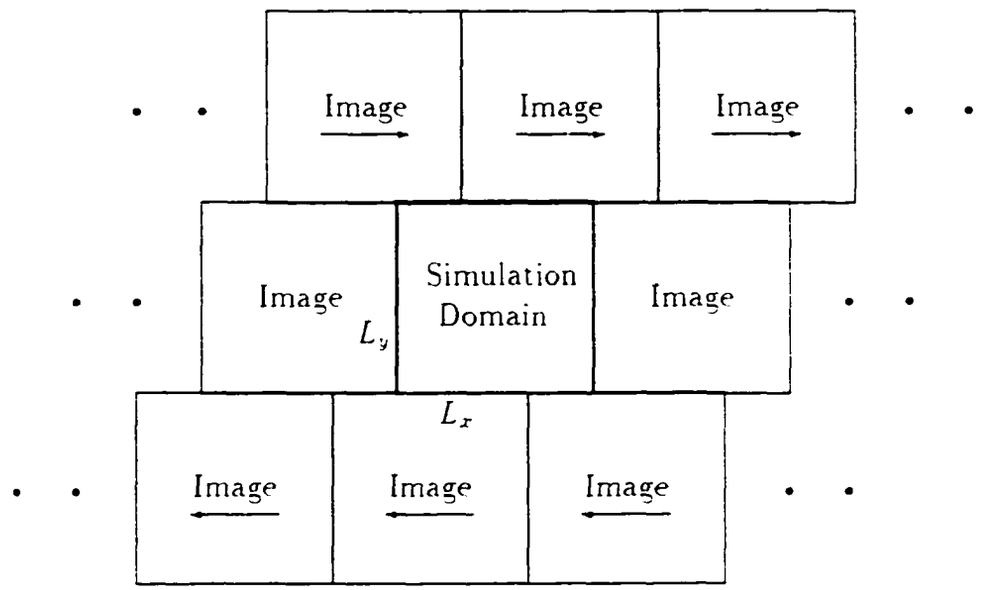

Figure 2.2: Simulation of a shear flow of particles in a domain following a periodic boundary condition. The image boxes mimic the conditions of simulation domain.

moved in x direction with a velocity v and those at the bottom moved in $-x$ direction with a velocity $-v$, the simulation domain experiences a constant shear rate equal to v/L_y. This is a so called periodic boundary condition and has been used widely for simulating shear flow of a granular material (Walton & Brown (1986); Campbell (1989); Hopkins & Louge (1990)). In addition for providing a means of conserving particles in the simulation domain, a periodic boundary condition provides an approximation to simulating a domain which is a part of an infinite region undergoing uniform shear flow.

For most part, the present simulation of granular phase is similar to that of Hopkins & Louge (1990). Table 2.1 is a comparison of the data for their steady state stresses in the flow with that in the present simulation in the absence of an agglomerate. Good agreement with their data (within 5% in most cases) is observed. The data corresponds to the simulation of smooth spherical two dimensional disks of uniform size in a square domain with an edge dimension equal to L. The letter ν in Table

Table 2.1: A comparison of the data for stresses in flow in present simulations in absence of an agglomerate with those in Hopkins & Louge (1990).

Conditions			Kinetic Stresses					
			Hopkins & Louge			*Present Simulations*		
ν	e	L/d_p	τ_{11}	$\tau_{12}=\tau_{21}$	τ_{22}	τ_{11}	$\tau_{12}=\tau_{21}$	τ_{22}
0.3	0.9	83	1.605	−0.420	1.374	1.673	−0.411	1.381
0.5	0.9	83	1.201	−0.264	1.119	1.252	−0.262	1.141
0.6	0.9	83	1.222	−0.222	1.166	1.361	−0.222	1.196

Conditions			Collisional Stresses					
			Hopkins & Louge			*Present Simulations*		
ν	e	L/d_p	τ_{11}	$\tau_{12}=\tau_{21}$	τ_{22}	τ_{11}	$\tau_{12}=\tau_{21}$	τ_{22}
0.3	0.9	83	1.522	−0.358	1.447	1.576	−0.379	1.496
0.5	0.9	83	3.500	−0.973	3.415	3.664	−1.012	3.567
0.6	0.9	83	6.352	−1.829	6.233	6.759	−1.951	6.648

2.1 denotes the solid fraction, e the coefficient of restitution, and L/d_p the ratio of the edge dimension L to the particle diameter d_p. The upper half of the table is a comparison for the kinetic component of the stress tensor, τ_k, which represents the momentum transfer due to the motion of particles between collisions, and the lower one is a comparison for the collisional component, τ_c, which represents the momentum transfer due to inter-particle collisions. The overall stress tensor, τ, is equal to $\tau_k + \tau_c$. For details on computations of τ_k and τ_c in the simulation model and for a further elaboration on the simulation in the granular phase, the reference is made to Hopkins & Louge (1990).

2.2.2 Agglomerate phase

In the present work a "wet agglomerate" phase has been introduced in the center of the simulation domain. In this phase the interstitial fluid is relatively dense and viscous (such as water or an organic binder fluid used in industrial granulation operations). The contribution of the interstitial fluid in momentum transfer cannot be ignored now. The resulting particle movement can be modeled by an approach known as Stokesian Dynamics (Brady & Bossis (1988)). In its most general form the particle motion in a fluid is modeled by the Langevin equation:

$$\mathbf{m}\cdot\frac{d\mathbf{U}}{dt} = \mathbf{F}^H + \mathbf{F}^P + \mathbf{F}^B \qquad (2.4)$$

where $\mathbf{m}$ is the generalized mass/moment-of-inertia matrix, $\mathbf{U}$ is the particle velocity vector, $\mathbf{F}^H$ is a vector of hydrodynamic force exerted on particles due to their motion relative to the fluid, $\mathbf{F}^P$ is the vector of deterministic nonhydrodynamic forces which may be interparticle ($\mathbf{F}^I$) or external ($\mathbf{F}^E$), and $\mathbf{F}^B$ is the vector of the stochastic forces that give rise to Brownian motion. For a suspension of particles of size greater than a micron in ordinary fluids such as water or air under normal conditions of temperature and pressure, $\mathbf{F}^B$ provides a negligible correction to particle velocity in

equation 2.4. Under the assumption that the contribution of $\mathbf{F}^B$ is negligible, that the external forces such as gravity are absent and that all particles are identical, spherical and smooth on their outer surface, the above equation reduces to:

$$m_p \frac{d\mathbf{U}}{dt} = \mathbf{F}^H + \mathbf{F}^I \tag{2.5}$$

where m_p is the particle mass and $\mathbf{F}^I$ represents the interaction forces between particles. We model the inter-particle interactions in the same manner as in the granular phase, i.e., the particles are taken as hard spheres having a constant coefficient of restitution which interact impulsively during a collision. Hence the particle motion *between* collisions follows the equation:

$$m_p \frac{d\mathbf{U}}{dt} = \mathbf{F}^H \tag{2.6}$$

Two important dimensionless parameters can be identified in the agglomerate phase. The particle Reynolds number (Re_p) is the ratio of fluid inertia to drag force due to the particle motion:

$$Re_p = \frac{\rho_{f_a} d_{p_a} U_a}{\mu} = \frac{\rho_{f_a} d_{p_a}^2 \dot{\gamma}}{\mu} \tag{2.7}$$

where ρ_{f_a} is the interstitial fluid density in the agglomerate and the characteristic particle velocity in the agglomerate phase, U_a, is again taken as $d_{p_a}\dot{\gamma}$. The particle Stokes number (St_p) is the ratio of particle inertia to the drag force experienced by it and hence can be expressed as:

$$St_p = \frac{\rho_{p_a} U_a^2}{\mu U_a / d_{p_a}} = \frac{\rho_{p_a} d_{p_a}^2 \dot{\gamma}}{\mu} \tag{2.8}$$

St_p is thus simply related to Re_p as: $St_p = (\rho_{p_a}/\rho_{f_a})Re_p$, and to the deformation

Stokes number, St_{def}, defined in equation 2.2 as: $St_p = (\rho_{pa} d_{pa}^2 / \rho_{pg} d_{pg}^2) St_{def}$. If the particles in the granular and agglomerate phase are identical, St_p is equal to St_{def}.

If $Re_p \ll 1$, the hydrodynamic force induced by the particles on the fluid, $-\mathbf{F}^H$, is related to the particle velocity $\mathbf{U}$ by the following linear relation (Happel and Brenner (1973)):

$$-\mathbf{F}^H = \mathbf{R}(\mathbf{x})(\mathbf{U} - \mathbf{U}^\infty) \tag{2.9}$$

where $\mathbf{U}^\infty$ is the fluid velocity in the absence of particles (and is equal to zero in the present case), and $\mathbf{R}$ is the resistance matrix, which depends only on the particle configuration $\mathbf{x}$. The Langevin equation 2.6 then reduces to:

$$St_p \frac{d\hat{\mathbf{U}}(\hat{t})}{d\hat{t}} = -18\hat{\mathbf{R}}(\mathbf{x})\hat{\mathbf{U}}(\hat{t}) \tag{2.10}$$

where the hats represent non-dimensional variables. Here $\mathbf{U}$ is non dimensionalized by $\frac{1}{2} d_{pa}$, t by $\dot{\gamma}^{-1}$ and the resistance matrix, $\mathbf{R}$, by the drag factor $3\pi\mu d_{pg}$. We wish to model the particle movement in the agglomerate by the above equation expressed in a finite difference form. If the time step of integration is kept small enough, $\mathbf{R}$ can be approximated by the identity matrix $\mathbf{I}$ since $\mathbf{R}$ is computed as a function of the particle configuration $\mathbf{x}$ at each step (Ichiki & Hayakawa (1995)). Under this approximation the above equation simplifies to:

$$\hat{\mathbf{U}}(\hat{t}) = \hat{\mathbf{U}}(0)\exp\left(-\frac{18\hat{t}}{St_p}\right) \tag{2.11}$$

From the above equation it is apparent that St_p is an important parameter governing the dynamics of particle movement in the agglomerate. When particles come very close to one another, short range lubrication forces become important and the present scaling of $\mathbf{R}$ breaks down. The present simulation does not capture this effect and

neglects the presence of the lubrication forces. However, as an approximation, we have taken the coefficient of restitution in the agglomerate phase as zero in an attempt to incorporate the effect of relatively large lubrication forces.

Since the agglomerate phase is freely suspended in the granular phase, the agglomerate as a whole will translate and rotate relative to the granular phase. The particle velocity vector in the agglomerate phase with respect to a fixed reference frame is thus:

$$\mathbf{U} = \mathbf{U}^A - \mathbf{U}^R \tag{2.12}$$

where $\mathbf{U}^A$ is the velocity of the agglomerate as a whole with respect to the fixed reference frame and $\mathbf{U}^R$ is the particle velocity in the agglomerate with respect to a reference frame fixed to the agglomerate. It is $\mathbf{U}^R$ that contributes to the Stokesian Dynamics calculations. The agglomerate velocity, $\mathbf{U}^A$, can be computed from the force/torque balance on the agglomerate. It can be written as: $\mathbf{U}^A = \mathbf{U}^A_T - \mathbf{U}^A_R$, where $\mathbf{U}^A_T$ is the translational and $\mathbf{U}^A_R$ is the rotational component. The translational component, $\mathbf{U}^A_T$, can be evaluated by considering the force balance:

$$m_a \frac{d\mathbf{U}^A_T}{dt} = \sum_i \mathbf{F}^H_i \tag{2.13}$$

where m_a is the mass of the agglomerate and can be estimated by modeling the agglomerate as having no interstitial fluid and having particles possessing an "effective enhanced mass", $\hat{m}_p$, due to the presence of interstitial fluid. $\hat{m}_p$ can be estimated as:

$$\hat{m}_p = \left(1 + \frac{\rho_{f_a}}{\rho_{p_a}} \left(\frac{1-\nu_a}{\nu_a}\right)\right) m_p = 3\, m_p \tag{2.14}$$

where ν_a is the solid fraction in the agglomerate and 3 is called as the mass en-

hancement factor. The agglomerate mass, m_a, is then equal to $N_a m_p$, where N_a is the total number of particles in the agglomerate. The rotational component of agglomerate velocity, $\mathbf{U}_R^A$, can be evaluated by considering the torque balance:

$$I_a \frac{d\omega}{dt} = \sum_i \hat{\mathbf{r}}_i \times \mathbf{F}_i^H \tag{2.15}$$

where I_a is the moment of inertia, ω the angular velocity and $\hat{\mathbf{r}}_i$ the position vector with respect to the center of mass of the agglomerate, and $\times$ denotes the vector cross product. The moment of inertia of agglomerate, I_a, can be estimated as:

$$I_a = \sum_i m_p (\hat{\mathbf{r}}_i \cdot \hat{\mathbf{r}}_i) \tag{2.16}$$

The rotational component of agglomerate velocity, $\mathbf{U}_R^A$, can then be computed as $\omega \times \hat{\mathbf{r}}_i$.

We now examine the effect of surface tension forces experienced by the particles at the outer surface of the agglomerate. Such forces, if significant, would tend to influence the deformed state of the agglomerate even when the forces inducing its deformation are absent (as in the case of a liquid drop which tries to regain its original spherical shape as soon as the forces inducing its deformation cease to exist). However, simple laboratory experiments show that a deformed wet agglomerate has no tendency to alter its state in the absence of forces inducing its deformation. We hence conclude that surface tension forces do not play a significant role in governing the dynamics of particle movement in the agglomerate and hence have neglected their effect in the present simulation.

We now examine the assumption $R\epsilon_p \ll 1$ by making an estimate of its highest possible order of magnitude under practical conditions. A typical high end shear rate employed in a granulation apparatus is of the order 10^2 sec.$^{-1}$. Taking an approximation of the largest particle size of powders granulated as 100 μm and taking

the interstitial fluid to be on the low end on the viscosity scale, such as water for example, we estimate the value of Re_p from equation 2.7 as 1. Most processes however, would employ lower shear rates, use binder fluids more viscous than water and granulate powders with a mean size of less than 100 μm. Hence we conclude that the assumption $Re_p \ll 1$ would be met under most practical conditions.

2.3 Simulation results

Table 2.2: Conditions for simulation corresponding to Figures 2.3, 2.4 and 2.5. Only input parameter changed in these figures is the deformation Stokes number, St_{def}.

Quantity	Value	Comments
L_x	1	Horizontal edge dimension of the simulation domain
L_y	1	Vertical edge dimension of the simulation domain
N	10,000	Number of particles simulated
ν_g	0.65	Solid fraction in the granular phase
ν_a	0.785	Solid fraction in the agglomerate phase
e_g	0.5	Coefficient of restitution in the granular phase
e_a	0.0	Coefficient of restitution in the agglomerate phase
α	2.0	Particle to fluid density ratio in the agglomerate
d_{p_g}	0.009127	Diameter of particles in the granular phase
d_{p_a}	0.009127	Diameter of particles in the agglomerate phase
d_a	0.20	Diameter of the agglomerate
f	0.02	Set point for av. fraction of particle dia. overlapped

Parameters chosen for the present simulation, except for the deformation Stokes number, St_{def}, are given in Table 2.2. Figure 2.3 is a picture of the simulation domain as it looks initially. Since particles are taken as spheres, the motion of which are restricted

to lie in a plane. Figure 2.3 provides a view which is normal to the plane containing these particles. The dark colored particles in the center represent the agglomerate, while the rest form the granular phase. Since particles in the granular and agglomerate phases are taken as identical, St_{def} is equal to St_p. Initial solid fraction (fraction of space occupied by solids in the plane containing the center of particles) in the agglomerate phase is set at the maximum value which can be sheared homogeneously in two dimensions, $\pi/4$ or 0.785 (Brady and Bossis (1985)). This high initial value is necessary to avoid an excessive "capture" of particles from the granular phase during the course of simulation. Initial solid fraction in the granular phase is taken as 0.65. Initial particle positions follow a regular square lattice arrangement and the center of mass of the system coincides with the center of the simulation domain. Particle velocities in the granular phase are initialized as the mean shear velocity superimposed on a small random component, in order to initiate collisions. Particle velocities in the agglomerate phase are initialized as zero. Initial particle velocities are readjusted slightly so that the initial net momentum of the domain is zero.

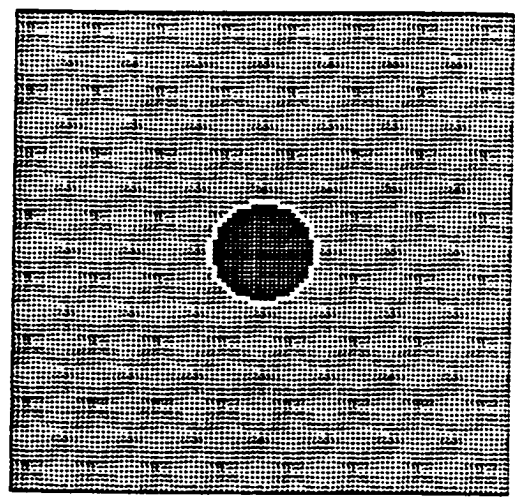

Figure 2.3: Snaphot of the simulation domain at zero dimensionless time units for conditions listed in Table 2.2.

As the simulation is allowed to proceed in time the agglomerate phase moves

relative to the granular phase and at times tends to come close to, or worse, leave the boundary of the domain. Since the image boundary conditions strictly hold only for a unidirectional flow (as would be the case in the absence of the agglomerate), the agglomerate must be kept as close to the center of the domain as possible so that the disturbance in the flow field created by its presence is not felt strongly at the top and bottom edges of the domain and the flow close to these boundaries is close to being unidirectional. In the present simulations the center of mass of the agglomerate is always kept at the center of the domain by making small adjustments to the overall momentum of the domain at each time step. Such an adjustment at each step in effect amounts to moving the "window" of the domain (which is used to observe the agglomerate in a region of infinite shear) such that the center of mass of the agglomerate occupies the center of the domain and thus should not affect any statistics or other results of the simulation except for the net momentum of the domain (which remains close to zero as a result of such an exercise). This conclusion has been verified by means of a few preliminary simulations.

Figures 2.4 and 2.5 show the time evolution of the domain for cases when St_{def} is equal to 0.018 and 0.18 respectively. The time in these figures is non-dimensionalized by multiplying with the shear rate. In Figure 2.4, where St_{def} is relatively low, the agglomerate elongates very little within 100 dimensionless time units. An increase in St_{def} by an order of magnitude in Figure 2.5, however, produces an appreciable deformation within this time. This result is in good agreement with experimental results (see next section) where a similar pattern of increase in the degree of elongation of agglomerates within a given time was observed as St_{def} of the system was increased. The experimental results also indicated that the deformed agglomerates become susceptible to breakage if the degree of elongation exceeds a particular value. Breakup of agglomerates occurs because at high elongations some particles are held together only by a few liquid bridges, which eventually rupture when stretched beyond a certain limit. Capturing this in simulation would require introduction of an appropriate rupture distance of a liquid bridge connecting two particles, and could be modeled based

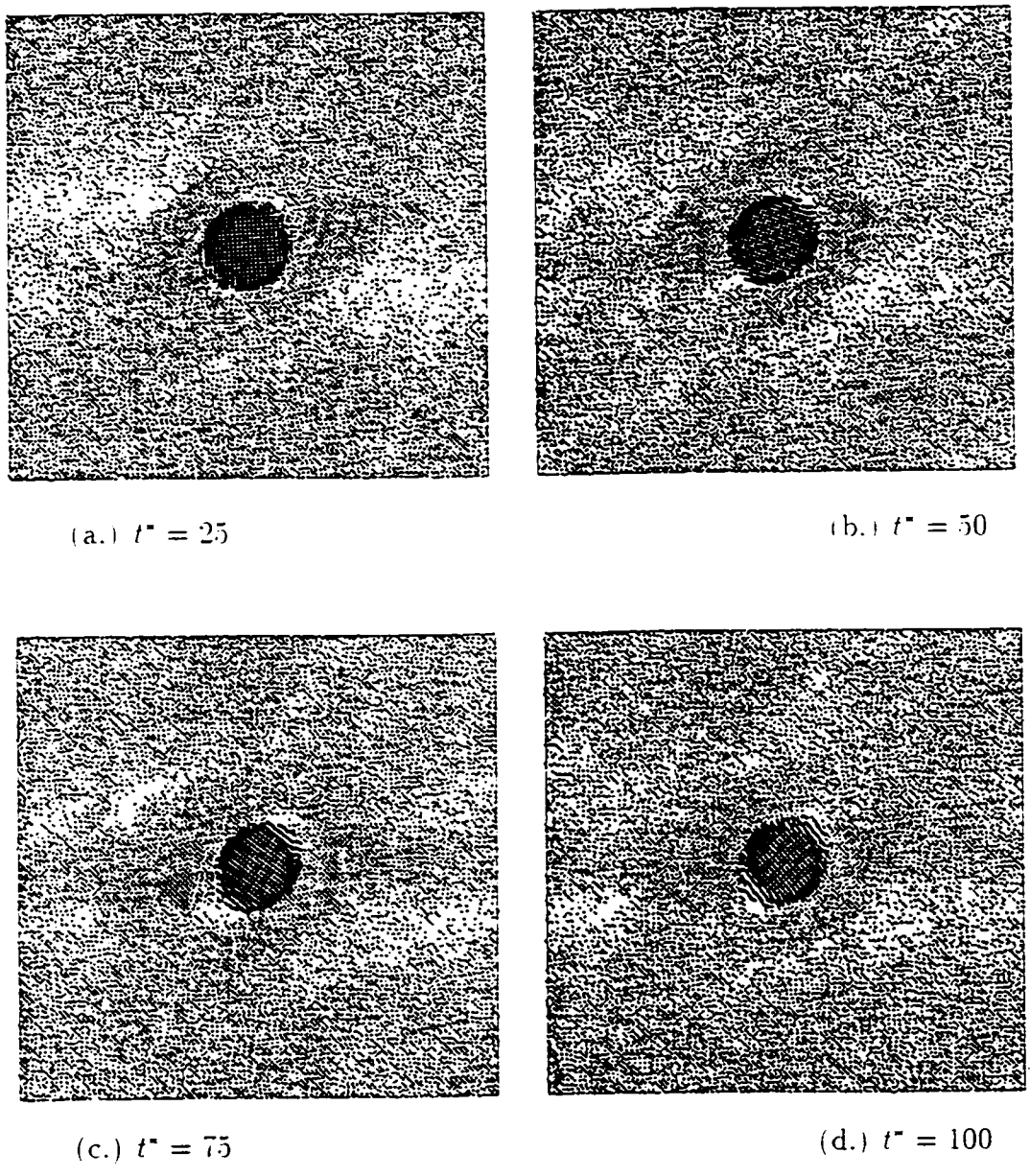

(a.) $t^* = 25$

(b.) $t^* = 50$

(c.) $t^* = 75$

(d.) $t^* = 100$

Figure 2.4: Snapshots of the simulation domain at (a.) 25, (b.) 50, (c.) 75 and (d.) 100 dimensionless time units for conditions listed in Table 2.2 and $St_{def} = 0.018$.

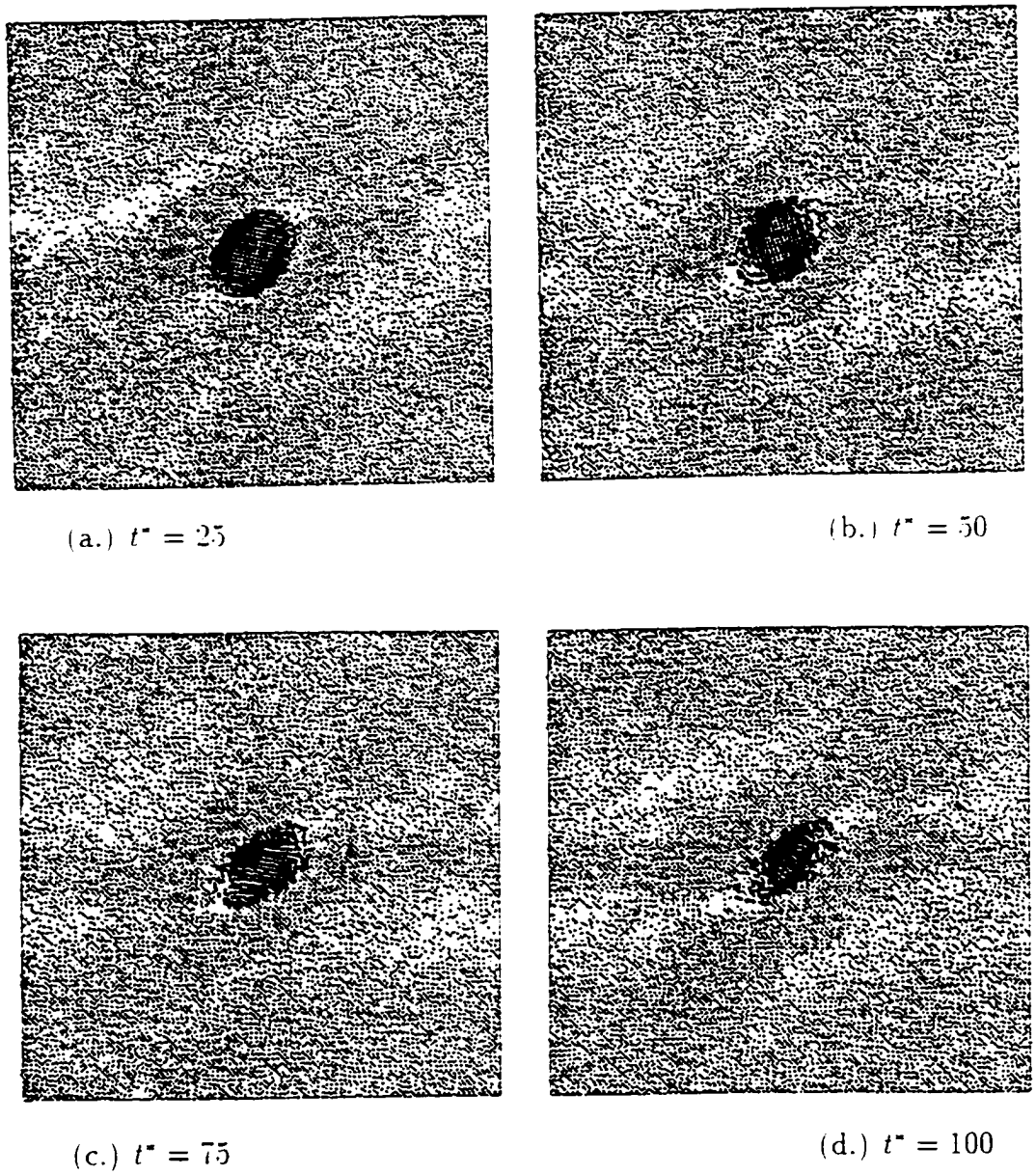

(a.) $t^* = 25$ (b.) $t^* = 50$

(c.) $t^* = 75$ (d.) $t^* = 100$

Figure 2.5: Snapshots of the simulation domain at (a.) 25, (b.) 50, (c.) 75 and (d.) 100 dimensionless time units for conditions listed in Table 2.2 and $St_{def} = 0.18$.

on an approach such as that described in Simons et al. (1994). The situation will be complicated however by the fact that the domain will then contain wet particles which are not confined to within a single agglomerate phase. The present simulation, hence, does not incorporate the phenomenon of liquid bridge rupture, and does not capture the phenomenon of agglomerate breakup into smaller pieces. However, by looking at the simulation domain, one can crudely judge if an agglomerate exists in a fractured state. For example, the last case in Figure 2.5 suggests that particles are chipped off at the two edges of the elongated agglomerate.

Figure 2.6 provides some insight into the mechanism of agglomerate deformation. Figure 2.6(a.) is a plot of the number of rotations of the agglomerate versus dimensionless time, t^*, (real time multiplied by the shear rate) for conditions listed in Table 2.2 and St_{def} equal to 0.018 (the rotation in the agglomerate is different from a pure solid body type rotation since an elongatory motion is simultaneously present). It can be concluded from this figure that the agglomerate rotates steadily with time, completing about 2 rotations in 150 dimensionless time units. The rate of rotation shows a slight decrease with time, a phenomenon that can be understood by considering Figure 2.7. This figure simply illustrates that a pure shear is composed of one half pure vorticity and one half pure strain. While a spherical agglomerate responds well to vorticity and rotates faster, an elongated one rotates slower and hence the decrease in the rotation rate as time progresses or as the agglomerate becomes more and more elongated. Figure 2.6(b.) is a plot of the orientation of the major axis (defined as the line joining the centers of particle pair farthest away from one another in the agglomerate) of the deformed agglomerate in degrees versus dimensionless time, where the angle is measured from the positive x-direction in a counter-clockwise direction. The orientation oscillates about a mean value of approximately 45 degrees, indicating that the elongated agglomerate tries to align itself in the direction of the straining component of the shear field (Figure 2.7). The nearly vertical jumps in Figure 2.6(b.) can be attributed to the sudden appearance of a particle pair forming a new major axis at an orientation angle greater than the current. The new major axis between these

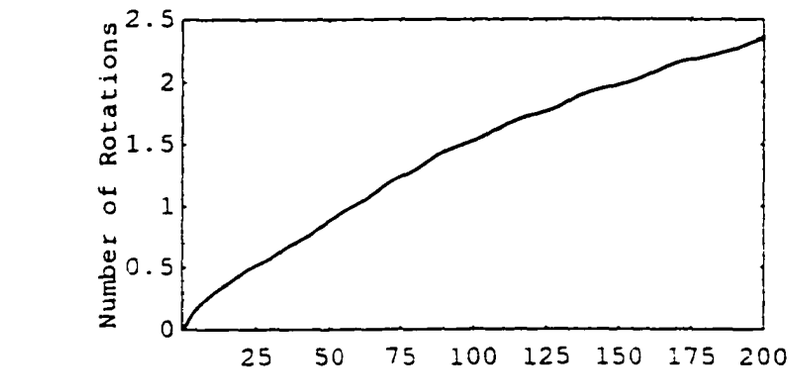

(a.)

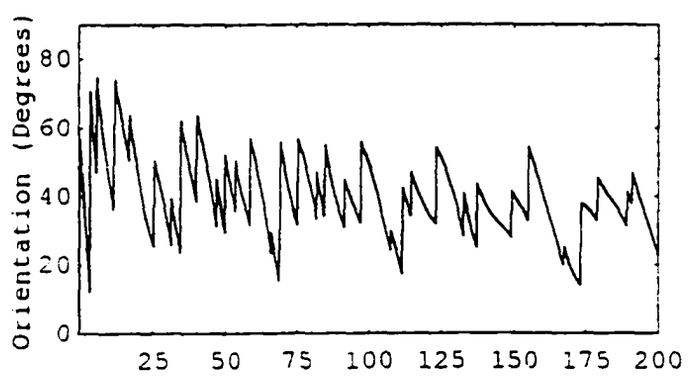

(b.)

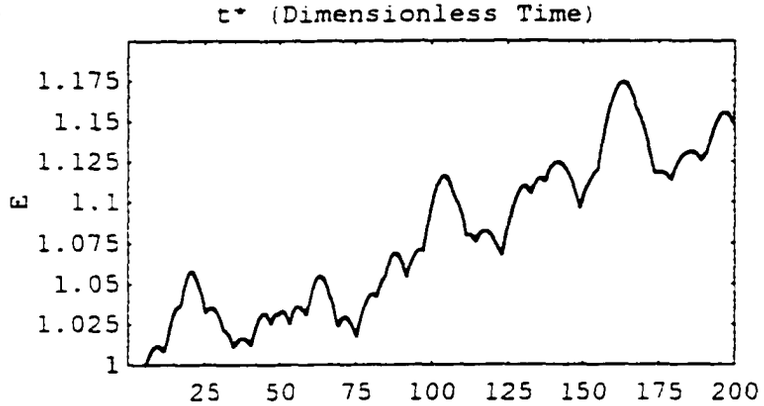

(c.)

Figure 2.6: (a.) Number of rotations of the agglomerate. (b.) Orientation of the major axis of the deformed agglomerate and (c.) Elongation parameter E versus the dimensionless time, t^*, for conditions listed in Table 2.2 and St_{def} equal to 0.018.

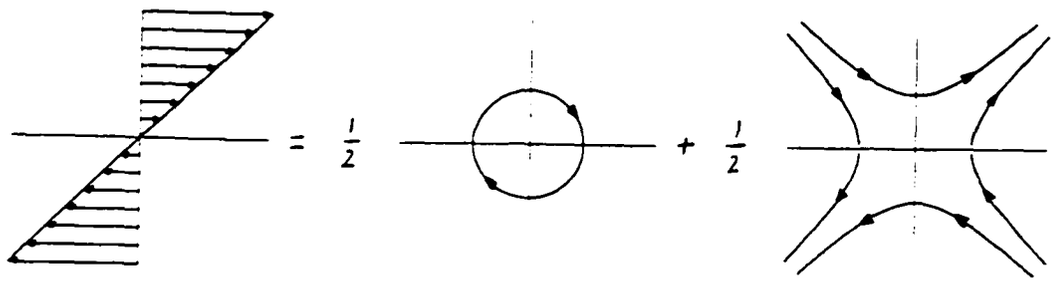

Figure 2.7: A pure shear field is composed of one-half pure vorticity and one-half pure strain.

particle pairs then rotates slightly with time (indicated by the slanted portions of the oscillations), decreasing the orientation until the sudden appearance of a new major axis. The period of oscillations also decreases with time indicating that elongated agglomerates have a greater tendency towards a sustained alignment in the direction of strain and a reduced tendency towards rotation than the more spherical ones; a conclusion that was also arrived at previously from observations of Figure 2.6(a.). Figure 2.6(c.) is a plot of the Elongation parameter E versus dimensionless time and shows that E increases with time, though not monotonically. The points of discontinuity in slope coincide exactly with the points of sudden jumps in Figure 2.6(b.), indicating that these are caused by the appearance of new particle pairs forming the major axis. As the agglomerate rotates, the major axis first increases in magnitude, which corresponds to the increasing portions of the plot in Figure 2.6(c.) and then decreases slightly, indicated by the decreasing portion. This decrease continues until the distance between another particle pair becomes large enough to become the new major axis. Over large time intervals E increases with time and the rate of elongation also increases, which again can be attributed to an increased response of an elongated agglomerate to the straining component of the shear field.

Figure 2.8 is a plot of the Elongation parameter, E, versus St_{def} for conditions listed in Table 2.2, and for different dimensionless time units. Each curve in Figure 2.8 is formed by joining 9 points obtained from several simulation results. Each point

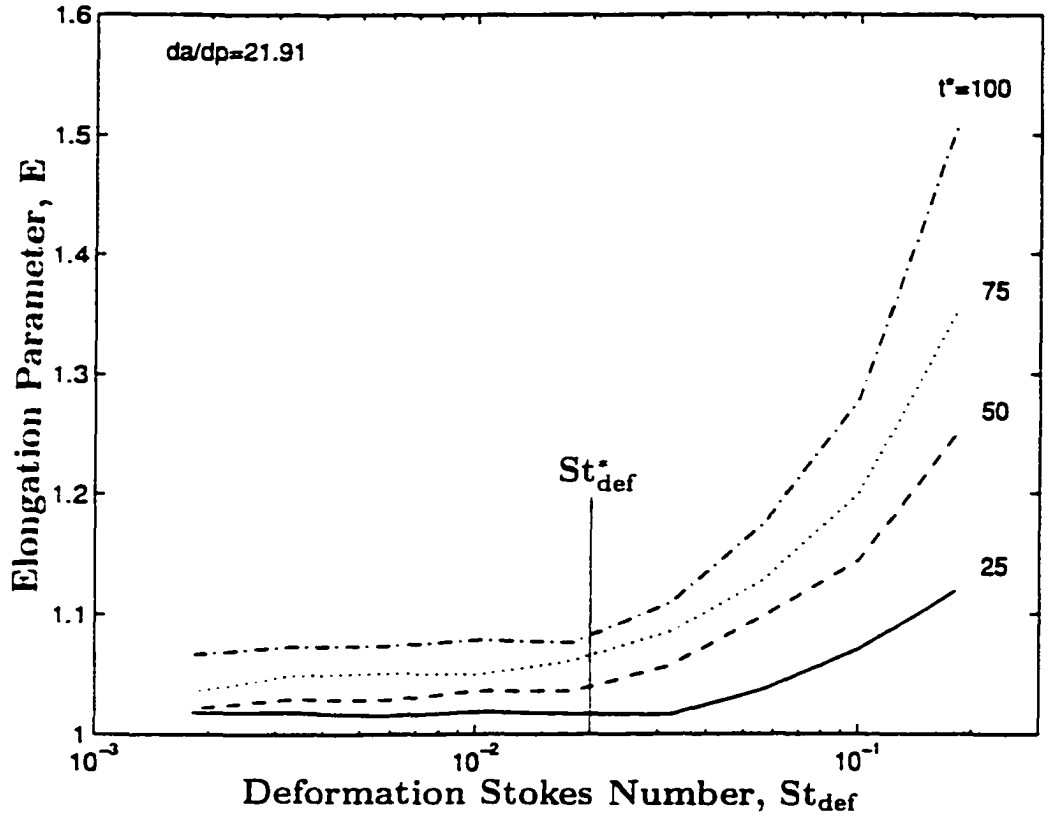

Figure 2.8: A plot of the Elongation parameter, E, versus the deformation Stokes number, St_{def}, for the conditions listed in Table 2.2 and for different values of dimensionless time units.

is itself an average of three obtained from different initial conditions. This averaging out over several points reduces the jagged nature of the plot and makes it smoother since it in effect serves to reduce the error in simulation. E is observed to increase with St_{def} as expected, for all times. An interesting feature of Figure 2.8 is the existence of two distinct regimes based on the value of St_{def} having relatively low and high characteristic values of E. We call the value of St_{def} which separates these two regimes, as the critical deformation Stokes number, St^*_{def}. The magnitude of St^*_{def} can be concluded from Figure 2.8 to be approximately 0.02. Since the rate of elongation for regions above St^*_{def} is significantly higher than that below, we can say that the agglomerates possess a much higher tendency towards deformation (and breakage) if the value of St_{def} lies above St^*_{def}. Thus St^*_{def} can be regarded as an important parameter characterizing the stability of the agglomerate. Which, as seen from the figure, is also relatively insensitive to variation in time for the simulated dimensionless time of 100 units.

We now explore the effect of changing the agglomerate diameter relative to the particle diameter on the simulation results. Figure 2.9 is a plot of E versus St_{def} for conditions listed in Table 2.2 and 100 dimensionless time units for different values of the relative agglomerate diameters (d_a/d_p). Each curve is again obtained by joining 9 points obtained from simulation results, each point itself being an average of three obtained from different initial conditions. The curve for small agglomerates is a little jagged since the error in simulation results decreases with the number of particles, N, as $1/\sqrt{N}$ (since the standard deviation of a collection of random variables decays with the sample size, N, as $1/\sqrt{N}$) and smaller agglomerates also contain fewer particles. The different values of (d_a/d_p) tested were 27.34, 21.91, 16.45 and 10.98. It is apparent from this figure that, for the range of (d_a/d_p) simulated, the value of St^*_{def} is nearly insensitive to variations in the relative agglomerate size, i.e., all agglomerates make a transition from the low to high elongation regime at nearly the same value of the critical St_{def} of approximately 0.02. However, for any given value of St_{def}, agglomerates having lower relative sizes possess a higher value of E. In other

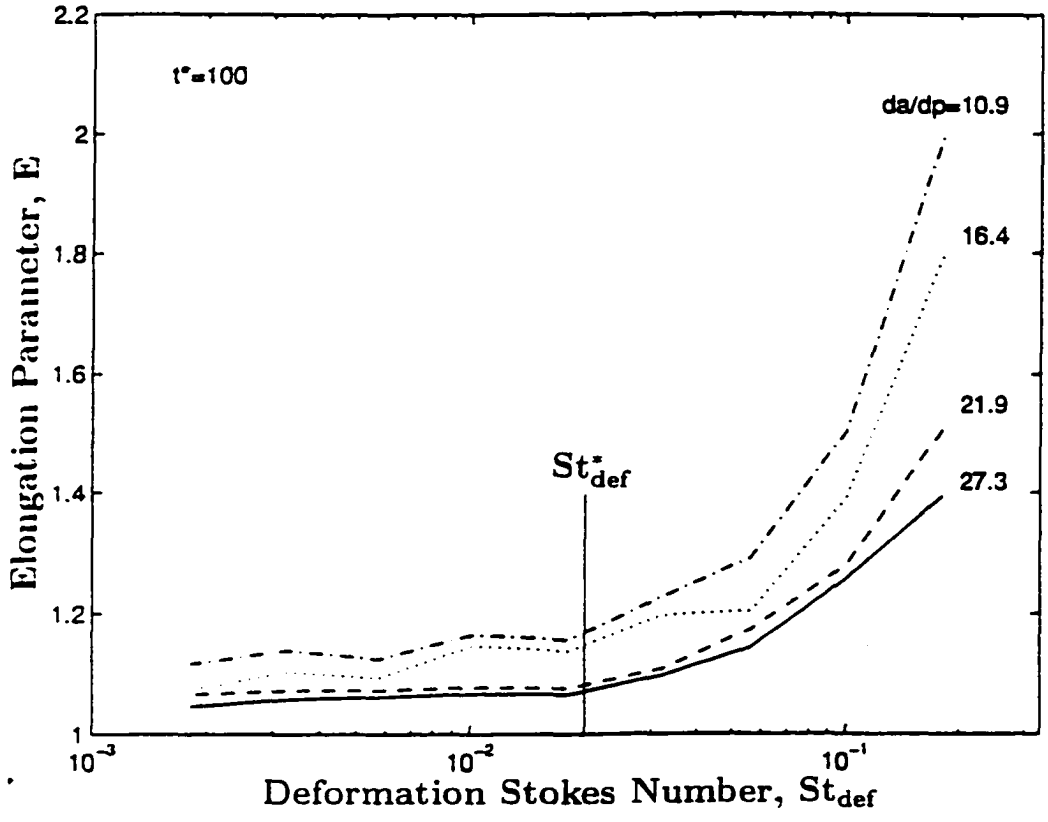

Figure 2.9: A plot of the Elongation parameter, E, versus the deformation Stokes number, St_{def}, for conditions listed in Table 2.2 and 100 dimensionless time units for different values of relative agglomerate diameters (d_a/d_p).

words, under similar conditions smaller agglomerates tend to be more unstable than larger ones. This relative unstable nature of smaller agglomerates might explain the reason behind the difficulty in obtaining stable nuclei (small agglomerates) during granulation (Pietsch (1996)).

2.4 Experiments

In order to test the conclusions reached from simulation results, experiments on deformation and breakup of agglomerates were performed. The primary requirement for such an experimental study is a setup in which a granular material can flow in a manner closely approximated by simple shear flow. For Newtonian fluids, the most common arrangement of this kind is a Couette device, which consists of two concentric rotating cylinders with fluid in the annulus; the thickness of annular gap being much smaller than the diameter of cylinders. Although granular materials do not behave as Newtonian fluids, and exhibit complex flow behavior (Campbell (1990)), an 'idealized' granular material in a zero gravity environment obeying no-slip boundary conditions at the walls develops a linear velocity profile along the shear gap. This behavior has been observed in computer simulations by Campbell & Brennen (1985). The idealized granular material used by these authors was one in which all particles were spherical, of equal size, having constant coefficients of restitution and surface friction, and which interacted only by means of instantaneous collisions. Such interparticle interaction is likely to be predominant in a real granular material when it flows fast, as in the 'grain-inertia' regime.

A common experimental technique with granular materials to obtain a no-slip boundary condition is to make the solid walls extremely rough (Savage & Syed (1984)). A simple way to obtain an approximate uniform shear flow of a granular material might then be to roughen the walls of a Couette device with sand paper of appropriate coarseness and then shear the material inside the annular gap. Such an exercise, however, would prevent the granular material from flowing in the grain-inertia regime.

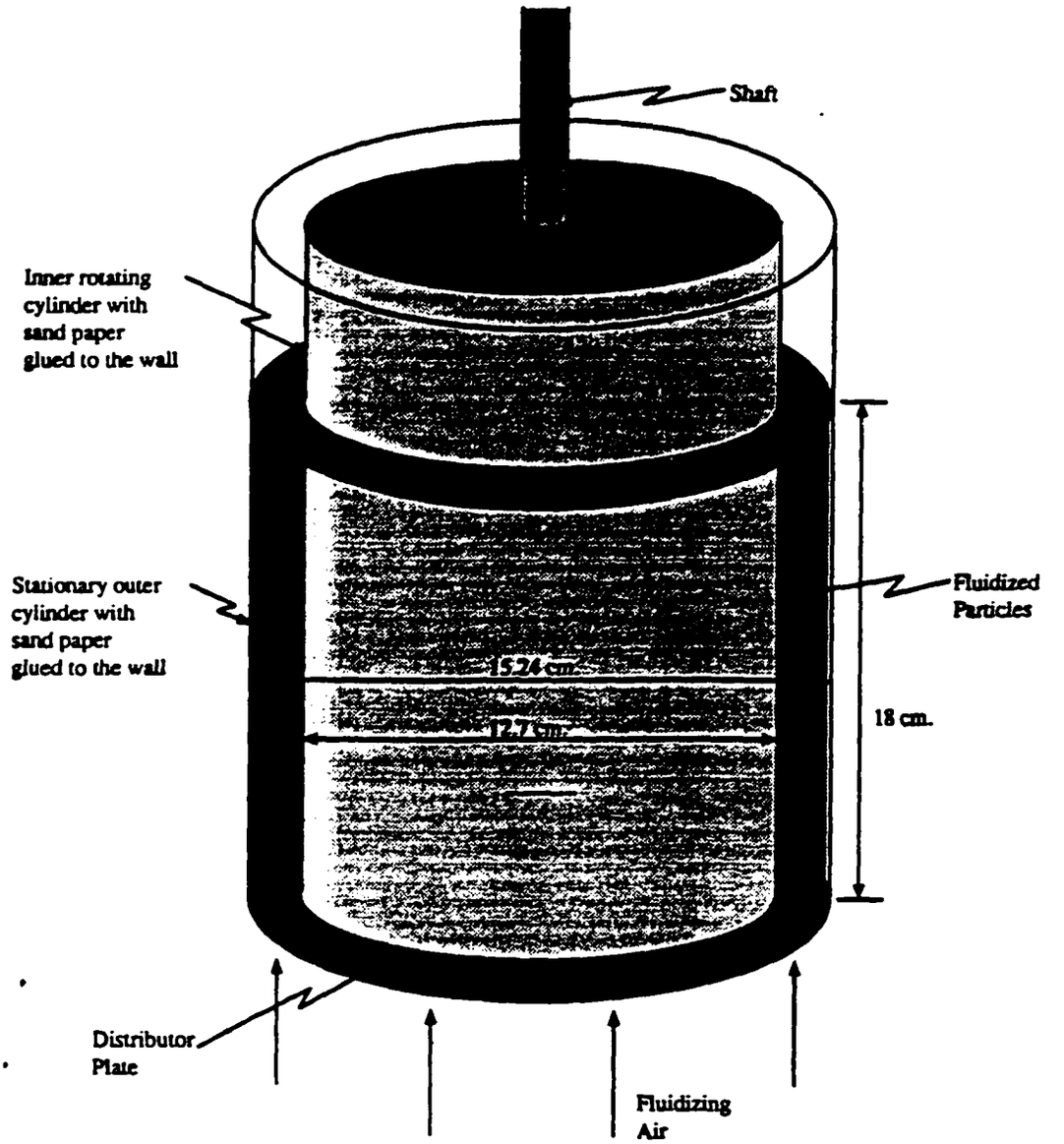

Figure 2.10: Schematic of the fluidized-bed granular-flow Couette device.

due to the presence of gravity (which acts along the axis of the cylinders), which increases the frictional interaction among adjacent layers in the direction of gravity. This frictional loading increases vertically down from the free surface of the granular material. This undesirable effect was eliminated in the present experiments by means of fluidizing the particles (Kunii & Levenspiel (1991)) with air entering at the bottom of Couette device. If the velocity of upflowing air is kept equal to the minimum fluidization velocity of particles, upward drag force on particles balances the downward force of gravity. The net force on individual particles is then zero, and frictional interaction among them is considerably reduced. The particles can then flow in the grain-inertia regime, provided that enough momentum is imparted to them by the moving walls. The detailed experimental setup utilized in this work is shown in Figure 2.10.

Experiments were performed with the fluidized-bed Couette device described above using glass particles of a mean size of about 300 microns such that 80% of the particles lay within the range of 350-250 microns. The density of particles was within the range of 2.42-2.5 gm/cc. Under Geldart's classification scheme (Kunii & Levenspiel (1991)), these particles classify as class B. The minimum fluidization velocity of the particles was found experimentally to be about 8 cm/sec. The volume fraction of bed at minimum fluidization conditions was estimated approximately as 0.4 (Kunii & Levenspiel (1991)). Sand paper was glued to the walls of the two cylinders as is shown in Figure 2.10. Its coarseness was chosen such that it was roughly equal to the size of glass beads. The bed was fluidized at minimum fluidization conditions and the inner cylinder rotated. Rotation at low speeds caused shear only in the particles close to the inner rotating cylinder. This was due to the fact that granular flows dissipate energy, and hence energy imparted by the moving wall had to exceed a certain threshold in order to cause flow across the gap. Shear penetrated the whole bed only for rotational speeds exceeding about 50 RPM. High rotation speeds (exceeding about 100 RPM) caused slip on the inner wall, due to a decrease in 'particle pressure', caused by an increase in the centrifugal forces experienced by the particles. Hence,

in all experiments, the rotational speed of the inner cylinder had to be kept between 50 and 100 RPM. The shear rate in the annular gap was estimated from the velocity of the inner cylinder and the thickness of the shear gap.

Wet agglomerates were formed in the Couette device kept at minimum fluidization conditions by adding droplets of an aqueous solution of 20 K Carbowax (Polyethylene Glycol) of known concentration using a syringe. The droplets of Carbowax solution quickly penetrated inside the bed of particles and formed wet agglomerates. If the bed was kept stationary while adding the droplets, the initial shape of wet agglomerates deviated slightly from spherical due to an uneven penetration of liquid. Shearing the bed at very low rates while adding the droplets helped in achieving an initial nearly spherical shape. The rate and time of shear during this exercise were kept low enough (at about 26 $sec.^{-1}$ and 30 sec. respectively) so that negligibly small elongations were produced. The technique worked well for the entire range of concentrations of Carbowax solutions used.

Experiments on deformation and breakup of wet agglomerates were performed in the following manner: The bed was fluidized at minimum fluidization conditions and ten initially spherical wet agglomerates were produced in the manner described above. Adding ten droplets of Carbowax solution to the bed took approximately 15 seconds. Subsequently, the rotation rate of the inner cylinder was increased to the desired value and held constant for a certain amount of time, characteristic of each experiment. During this time the wet agglomerates deformed to various degrees depending upon the experimental conditions. The rotation rate was then reduced to zero and the bed kept stationary at minimum fluidization conditions for several more minutes. During this time the deformed state of the wet agglomerates was preserved while they slowly dried. The required drying time under these conditions, for the range of concentrations of Carbowax solutions used, was found to be about 50 minutes. Dry agglomerates were then carefully sieved and the Elongation parameter, E, determined by measuring the major axis manually using a projection microscope.

Two sets of experiments were performed: One in which the variation of Elongation

Table 2.3: Experimental results for the variation of Elongation parameter, E, with time for a fixed value of deformation Stokes number, $St_{def} = 0.013$.

Time (minutes)	Elongation Parameter (E)	m_a/m_a^2	Number Unbroken
1	1.11	1.11	10
2	1.17	1.11	10
3	1.16	1.06	10
4	1.18	1.09	10
5	1.24	0.96	10
6	1.29	1.03	10
7	1.30	1.01	10
8	1.32	0.99	10
9	1.36	0.96	9
10	1.33	0.96	7
11	1.35	1.03	7
12	1.41	0.98	6
13	1.47	1.00	7
14	1.50	0.99	4
15	–	–	0

Table 2.4: Experimental results for the variation of Elongation parameter, E, with deformation Stokes number, St_{def}, for a fixed run time of 5 minutes.

Viscosity of Carbowax Solution (kg/m sec.)	Shear Rate (1/sec.)	Deformation Stokes Number (St_{def})	Elongation Parameter (E)	m_a/m_a^v	Number Unbroken
7.82	31.41	0.000889	1.07	1.22	10
4.52	39.26	0.001923	1.14	1.21	10
2.41	45.55	0.004174	1.18	1.18	10
1.19	49.21	0.009108	1.33	1.14	10
0.54	49.21	0.019839	1.38	1.03	10
0.23	45.55	0.043087	1.32	0.92	6
0.09	39.26	0.093804	–	–	0

parameter, E, with time was studied for a fixed value of the deformation Stokes number, St_{def}. In the other set the variation of E with St_{def} was studied for a fixed time. The deformation Stokes number, St_{def}, was held constant during the first set of experiments by holding constant the rotation rate of the inner cylinder (which determines the shear rate, $\dot{\gamma}$), and the concentration and temperature of the 20 K Carbowax solution (which influences its viscosity, μ). Actual values of shear rate and viscosity were 34 sec.$^{-1}$ and 0.55 kg/m sec., respectively. The particle size, d_{p_j}, and density, ρ_{p_j}, for the glass particles were taken as their mean values provided by the supplier as 300 μm and 2.46 gm/cc, respectively. The value of St_{def} during these set of experiments was thus estimated from Equation (2) as 0.013. Several experiments with run times varying from 1 to 15 minutes, with an increment of 1 minute, were performed (see Table 2.3). During the second set of experiments, run time was fixed at 5 minutes. The deformation Stokes number, St_{def}, was varied in these set of experiments by varying both the rotation rate of the inner cylinder and the concentrations of 20 K Carbowax solution. Seven experimental runs were performed

with values of St_{def} varying between 0.0008 and 0.0938 (see Table 2.4).

In order to quantify agglomerate breakage (see last column in Tables 2.3 and 2.4), the mass of a dry deformed agglomerate, m_a, was compared to its mass at zero time, m_a^*. The mass at zero time, m_a^*, was estimated by forming ten wet agglomerates in the Couette device, imparting an initial spherical shape to them by the method discussed previously, drying them in that state without any further shearing, and measuring their average mass (the diameter of the original undeformed agglomerate, d_a, was estimated by measuring the average diameter of these agglomerates in two perpendicular directions and then taking their average). Under conditions of low deformation, m_a exhibits a slight increase (about 10% on an average) over its zero shear mass, m_a^* (see before last column in Tables 2.3 and 4). This phenomenon can be attributed to the capture of particles by the agglomerate from surrounding granular material when it is sheared. The effect of agglomerate breakage, on the other hand, tends to reduce the dry agglomerate mass, m_a, either as result of chipping of individual particles from the ends along the major axis, or as a result of its fragmentation into two or more agglomerates. A dry agglomerate is thus (quite arbitrarily) considered as "broken" if its mass, m_a, is less than 90% of its corresponding mass at zero time, m_a^*. The last column in Tables 2.3 and 2.4 reports the number of unbroken agglomerates, out of the initial ten, as determined by this criteria. The second last column in Tables 2.3 and 2.4 lists the average ratio m_a/m_a^* measured over the unbroken agglomerates. Measurements of the Elongation parameter, E, are also reported as averages over the unbroken agglomerates.

Figure 2.11 displays experimental results for the variation of Elongation parameter, E, with time for a fixed value of $St_{def} = 0.013$. Some samples of dry deformed agglomerates are placed vertically above data points to which they correspond. The Elongation parameter, E, is observed to increase with time. The behavior is in good qualitative agreement with that of the 'smoothed-out' behavior of Figure 2.6(c.), which displays the simulation results for the variation of E with time, for a fixed value of $St_{def} = 0.018$. The Elongation parameter, E, acquires a value of about 1.1

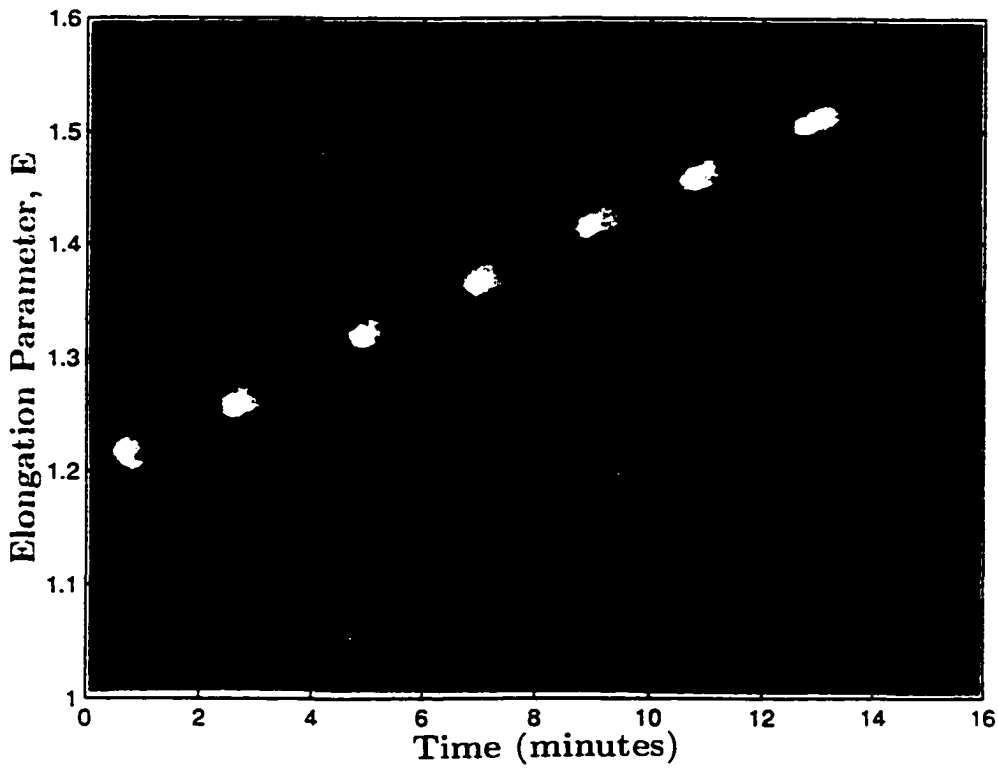

Figure 2.11: Variation of the Elongation parameter, E, with time for a constant value of deformaton Stokes number, $St_{def} = 0.013$.

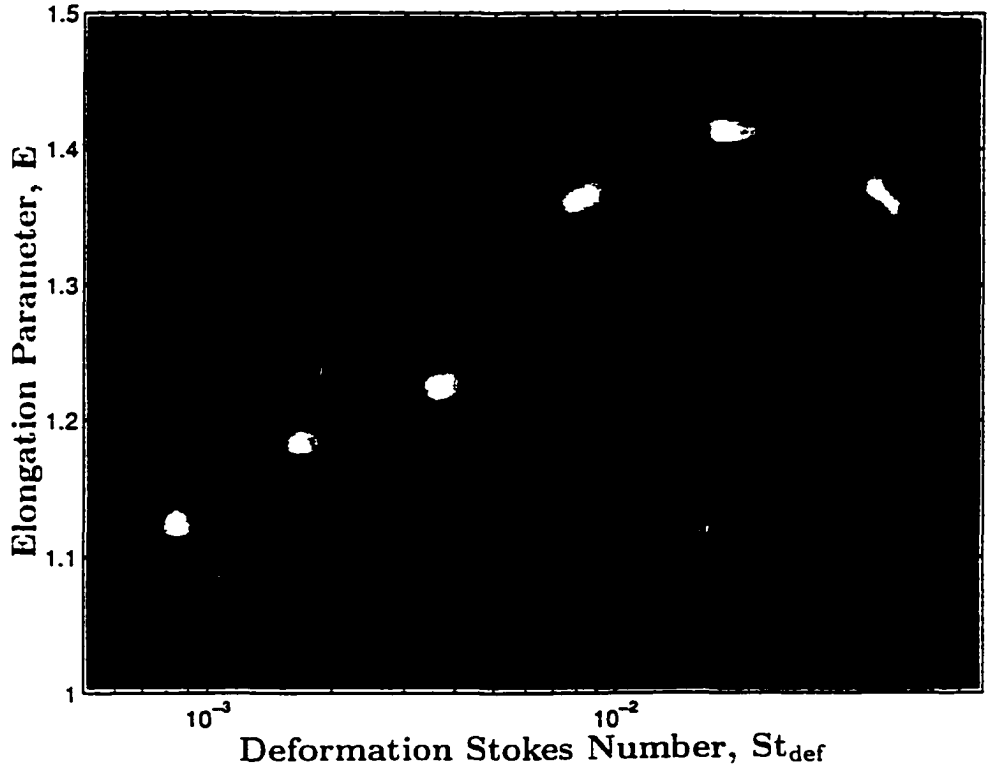

Figure 2.12: Variation of Elongation parameter E with the deformation Stokes number, St_{def}, for a constant time of 5 minutes.

in 1 minute and increases to a value of about 1.5 in 14 minutes. Partial breakage of agglomerates (only some of the original ten surviving) is observed for all times exceeding 8 minutes. The fraction of broken agglomerates increases with time, and all agglomerates break during the experiment with a run time of 15 minutes.

Though the values of St_{def} in experimental and simulation conditions of Figures 2.11 and 6(c.) are close, there is a substantial disparity in run times. The simulation run time in Figure 2.6(c.) is 200 dimensionless units, whereas the experimental one in Figure 2.11 ranges from about 2042 to 28588 dimensionless units (from 1 to 14 minutes). Much larger run times are required in actual experiments since variations in Elongation parameter, E, can be measured accurately over small time increments in simulations but cannot be measured accurately in experiments, due to the presence of experimental "noise". Meaningful data in experiments can be gathered only over time increments of about 1 minute, which, at the experimental conditions in the apparatus, corresponds to about 2042 dimensionless time units.

Figure 2.12 displays experimental results for the variation of the Elongation parameter, E, with the deformation Stokes number, St_{def}, for a fixed run time of 5 minutes. Samples of dry deformed agglomerates are again placed vertically above the data points to which they correspond. The Elongation parameter, E, is observed to increase with St_{def}. The two regimes of low and high characteristic deformation are also apparent. The behavior is again in good qualitative agreement with that of Figures 2.8 and 2.9, which display the simulation results for the variation of E with St_{def} for various dimensionless time units and relative agglomerate diameters (d_a/d_p). Values of the relative agglomerate diameter, (d_a/d_p), ranged in simulations from about 10.9 to 27.3, while during experiments from about 16.8 (for an agglomerate made of 50% Carbowax solution) to about 22.6 (for an agglomerate made of 25% Carbowax solution).

The lower limit of St_{def} in Figure 2.12 is chosen such that a sufficiently low value of E is obtained within the given experimental run time. The increment in the value of St_{def}, by a factor of $10^{1/3}$ between two successive data points, is again chosen

such that a clear pattern of change in E with St_{def} is observed. The upper limit is determined by the lowest possible concentration of Carbowax solution which can still make agglomerates strong enough so that they do not break easily during handling. Run time of 5 minutes is taken such that for the chosen range of St_{def}, agglomerates in the high elongation regime acquire a sufficiently high elongation without breaking.

A quantitative comparison of the values of the critical Stokes number, St^*_{def}, in experiments and simulation can be made despite the fact that simulations and experiments cover different time ranges, since St^*_{def} was observed in Figure 2.8 to be relatively insensitive to the variations in time. The value of St^*_{def} from experimental results of Figure 2.12 is estimated approximately as 0.006. The same critical value estimated from simulation results in Figures 2.8 and 9 was found to be approximately 0.02. The discrepancy is surprisingly small considering experimental error, the large number of assumptions in the simulation model and the fact that the simulation is two dimensional while the experiments are not. Partial breakage of agglomerates is observed for the run corresponding to $St_{def} = 0.043$ ($St_{def} > St^*_{def}$). A run corresponding to $St_{def} = 0.093$ ($St_{def} \gg St^*_{def}$) resulted in a breakage of all agglomerates, as expected.

2.5 Conclusions

In addition to providing an insight into the phenomenon of shear induced agglomerate deformation and breakup, an important finding of this chapter has been that this phenomenon can be characterized by St_{def}, a parameter which represents a ratio of inducing (inertial) to resisting (viscous) forces, and which is also similar to the concept of St_b introduced in the previous chapter. We also found that there exists a critical value of this parameter, St^*_{def}, below which the forces inducing the deformation and breakage are low and above which they are high. This critical value was found to be relatively insensitive to some parameters of the system, and we concluded that it could be a constant for a given system, thus also supporting our hypothesis of the

constant nature of St_b^* in chapter 1. Relating St_{def} and St_b in a mathematical sense however has proved difficult due to nature of their distinctions mentioned in section 2.1.

It is also interesting to compare the present study with that of shear induced deformation and breakup of viscous drops in viscous fluids (Stone (1994)). A drop of viscous fluid when suspended in another viscous fluid undergoing shear flow exhibits a phenomenon identical to that observed in the present study: that of deformation by stretching. In both cases stretching occurs in the direction of the straining component of the shear field (Figure 2.7). Whereas the straining component causes the drop/agglomerate to elongate, vorticity in the flow serves to reduce the elongation. In the case of a drop, steady deformed shapes are possible since the surface tension effects drive the flow back into the drop and thus always try to make the drop spherical again. When the outer flow is stopped, the drop would regain its original spherical shape. However, steady deformed shapes in case of agglomerates are not possible because surface tension effects at the interface are negligibly small and there is no force which acts to make an elongated agglomerate spherical again. The mode of fragmentation in the two cases is also different. In case of a drop, fragmentation of an elongated drop occurs due to an instability in flow, and is caused by surface tension effects. Fragmentation of an elongated agglomerate is caused as a result of narrowing of its smaller dimension to a size comparable to that of the individual particles, and a subsequent rupture of liquid bridges which tend to hold them together.

A better quantitative comparison of the simulation results with experiments requires improvements in the experimental setup and/or a larger CPU time for simulations. A better experimental setup, with larger cylinder diameters to yield reduced curvature effects and one with a better speed control over the rotation of inner cylinder, would serve to reduce the experimental noise. This would allow a collection of data at smaller increments of time and St_{def}, thus also allowing lower total run times. This would hence make possible comparisons with simulation results at lower times much easier. An increase in the simulation run time on the other hand is limited

by the available CPU time. A simulation of 100 dimensionless time units in the present simulation with 10,000 particles required about 3 hours of CPU time on a SGI Power Challenge workstation using a MIPS R8000 processor. Thus a simulation run for a time comparable to the *smallest* experimental run time (1 minute or 2042 dimensionless time units) would require about 61 hours (2.5 days) of CPU time.

Relaxing the assumptions made in the simulation model also have implications of requiring larger CPU times. Consider an extension of the present simulation to three dimensions. Assuming a similar particle number density in three dimensions requires a simulation with about 10^6 particles. Since the computational algorithm for N number of particles is $O(N)$ (computation in both granular and agglomerate phases is $O(N)$), a simulation of 100 dimensionless time units on a similar machine would require about 300 hours (12.5 days) of CPU time. Reducing the number of particles would reduce the CPU time but would also increase the error in computation, thus requiring many simulation runs in order to reduce the error. Another appropriate extensional work would be to incorporate the effect of lubrication forces in the agglomerate phase, which were neglected in computing the dynamics of particle movement in the agglomerate in section 2. Computational demands of such an extension are even more severe, since the incorporation of lubrication forces is a costly $O(N^3)$ operation. If we assume that on an average 10% of particles are occupied by the agglomerate phase, incorporation of lubrication forces in the present simulations would increase the CPU time to about $3((9000 + 1000^3)/10,000)$ or 3×10^5 hours.

Despite its limitations, the present simulation model has provided a neat description of the process, both qualitatively and quantitatively. Moreover, the experiments have confirmed the qualitative conclusions reached from the simulation results. Together, the simulation and experiments, have led to a much better understanding of the phenomenon of shear induced deformation and breakup of wet agglomerates.

Chapter 3

A simulation of wet granulation and future work

In this chapter we redirect our focus to model the granulation problem directly by simulating shear flows of solid particles which are wet on their outer surface. Hence in principle the only additional consideration that one has to deal with compared with the simulation model of dry particles developed in the previous chapter is a proper incorporation of forces that the individual particles experience when they interact via the wet layers on their outer surface. The simulation serves as a complete model of the wet granulation process, in which agglomerate properties like their size, shape, and density can be inferred from the input parameters of the system, and if enough simulations can be performed these properties can be correlated with the input parameters in the range of operating conditions of interest.

It is known from simulations of shear flows of dry granular materials that a finite dissipation during inter-particle collisions (*i.e.* a restitution coefficient of less than unity) results in a slight tendency towards particle clustering (Hopkins and Louge (1990)). These clusters, however, do not act as stable entities and there is a continuous migration of particles in and out of the clusters. They also do not posses any 'strength', since they in effect are only a collection of closely spaced dry particles.

Tendency towards particle clustering increases with increasing surface dissipation (*i.e.* with a decreasing restitution coefficient). Figure 3.1 shows steady state snapshots of the simulation domain containing a shearing dry granular material with restitution coefficients of 0.9 and 0.0. The model of simulation is the same as that discussed in the previous chapter. The number of particles in the domain is 40,000 and the solid fraction is 0.4. The square box in the center represents the computed domain while the surroundings include particles in the periodic cells. The case with restitution coefficient, $\epsilon = 0.9$ shows a more or less uniform particle density throughout the domain while the one with $\epsilon = 0.0$ shows a tendency towards particle agglomeration.

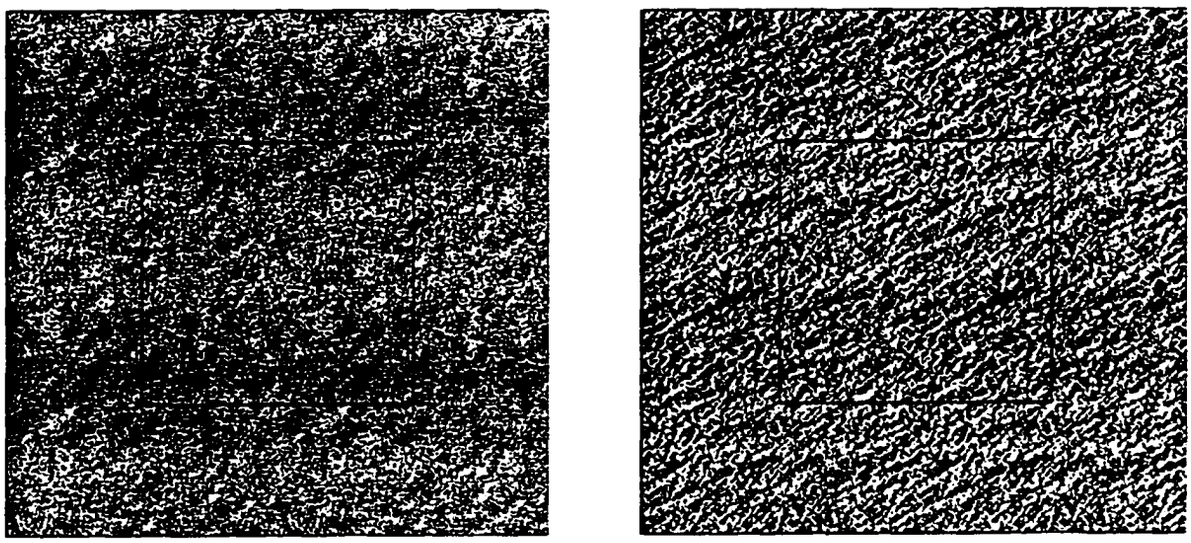

(a.) $\epsilon = 0.9$ (b.) $\epsilon = 0.0$

Figure 3.1: The effect of surface dissipation on particle clustering: Part (a.) is the snapshot of the simulation domain containing a shearing dry granular material at steady state with a restitution coefficient, $\epsilon = 0.9$, while part (b.) shows the case with $\epsilon = 0.0$.

The phenomenon illustrated in Figure 3.1 has some resemblance to particle agglomeration in wet granulation. We are hence encouraged to modify the simulation

Chapter 2 to simulate shear flows of particles which are wet on their outer surface. We hope to see in this simulation, particle agglomerates, the properties of which are a function of the input parameters of the simulation. In the following sections we present two models, each with a different mode of viscous interaction between particles interacting via their wet layers. We first present a simple model which considers forces only in the centerline direction and ignores lubrication effects. In the next section we refine this model to incorporate lubrication effects in the centerline direction.

3.1 The model with centerline forces and no lubrication effects

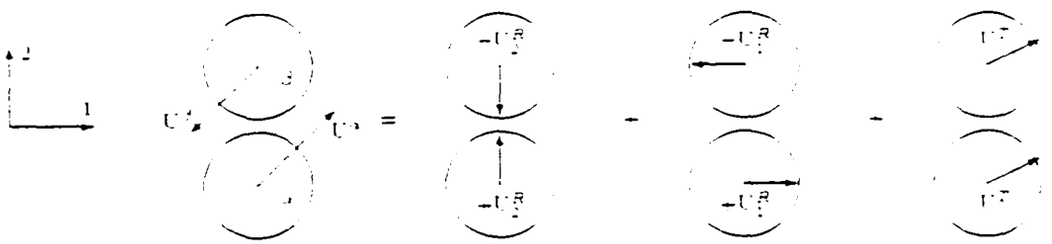

Figure 3.2: Breakdown of an arbitrary translational motion of two particles α and β past one another into purely relative and common translational components.

As a starting point, we model the viscous forces experienced by two particles interacting via their viscous wet layers as being dependent only on and proportional to their centerline relative velocity of approach. If $\mathbf{U}^{\alpha}$ and $\mathbf{U}^{\beta}$ denote the velocities of particles α and β respectively (Figure 3.2), we define a relative velocity of their approach as $\mathbf{U}^{R} \equiv 0.5(\mathbf{U}^{\alpha} - \mathbf{U}^{\beta})$. If $\mathbf{U}^{T} \equiv 0.5(\mathbf{U}^{\alpha} + \mathbf{U}^{\beta})$ defines a common translational, center of mass, velocity of the two particle system, then $\mathbf{U}^{\alpha} = \mathbf{U}^{T} + \mathbf{U}^{R}$ and

$\mathbf{U}^{\beta} = \mathbf{U}^{T} - \mathbf{U}^{R}$. In other words, the two particles at any instant can be thought of as moving with a common translational velocity of $\mathbf{U}^{T}$, and at the same time moving relative to one another with equal and opposite velocities equal to $\mathbf{U}^{R}$ (particles α and β with velocities equal to $+\mathbf{U}^{R}$ and $-\mathbf{U}^{R}$ respectively).

Let axis 2 point along the direction from the center of particle α to that of particle β, and axis 1 point along the direction perpendicular to 2 such that 1 and 2 form a right handed coordinate system. If U_1^R and U_2^R denote the components of $\mathbf{U}^R$ along directions 1 and 2 respectively, then the two particles move at any instant relative to one another with equal and opposite velocities equal to U_2^R along direction 2 and with U_1^R along direction 1. If the two particles interact via the wet layers over their surface, viscous forces will be experienced by them along directions 1 and 2 (the common translational motion will not contribute to any force). If direction 3 points outwards from the 1-2 plane, such that 1, 2 and 3 form a right handed coordinate system, torques will also be experienced by the two particles along direction 3.

If the wet layers are thin, i.e. if $h/d_p \ll 1$, where h is the thickness of the wet layer and d_p is the particle diameter, *lubrication effects* will dominate the viscous forces between two particles (provided also that the Reynolds number $Re \ll 1$, which we assume here and was shown in chapter 2 to be a good assumption under most practical situations). The dominant force is then directed along direction 2 while the one along direction 1 and torque along direction 3 are relatively weak. More rigorously, if $\xi = 2(R - d_p)/d_p$ defines a dimensionless gap width between the two particles, where R is the distance between their centers, the force along direction 2 is $O(\xi^{-1})$ to a leading order, while the one along direction 1 and also the torque along direction 3 are $O(\ln \xi^{-1})$. The centerline force thus far exceeds other effects under the limit $\xi \ll 1$. In this section we will consider only the centerline force and will model it in a simplified fashion. If $\mathbf{F}^{\alpha}$ and $\mathbf{F}^{\beta}$ denote the viscous forces experienced by particles α and β respectively, we model their components along the centerline direction 2 simply as:

$$F_2^\alpha = -3\pi\mu d_p U_2^R = -F_2^\beta \tag{3.1}$$

where μ is a constant and is only an approximation of the viscosity of the fluid in the wet layer. The component of $\mathbf{U}^R$ along direction 2, U_2^R, can be evaluated as $U_2^R = \mathbf{U}^R \cdot \mathbf{k}$, where "$\cdot$" denotes the vector dot product and $\mathbf{k}$ denotes a unit vector along direction 2. It can be evaluated as $\mathbf{k} = (\mathbf{r}^\alpha - \mathbf{r}^\beta)/|\mathbf{r}^\alpha - \mathbf{r}^\beta|$, where $\mathbf{r}^\alpha$ and $\mathbf{r}^\beta$ denote the position vectors of particles α and β respectively, and the denominator represents the magnitude of $(\mathbf{r}^\alpha - \mathbf{r}^\beta)$. The above equation can also be rewritten as:

$$F_2^\alpha = -\frac{18\dot{\gamma}\, m_p}{St} U_2^R = -F_2^\beta \tag{3.2}$$

where $St = \rho_p d_p^2 \dot{\gamma}/\mu$ is the Stokes number, ρ_p is the particle density and m_p is the particle mass. Since the simulation proceeds over small time steps, the above forces can also be expressed as: $F_2^\alpha = m_p(\bar{U}_2^R - U_2^R)/\Delta t = -F_2^\beta$, where U_2^R now denotes the initial centerline relative velocity before the time step, $\bar{U}_2^R$ denotes its final value after a time step, and Δt denotes the magnitude of the time step. The magnitude of the centerline relative velocity in equation 3.2 can be approximated by any value acquired by it during a time step. If it is approximated by the initial value, U_2^R, the expression for force remains same as that in equation 3.2, while if it is approximated by the final value, $\bar{U}_2^R$, the equation can be rearranged to yield the following expression for force in terms of the initial velocity, U_2^R:

$$F_2^\alpha = -\frac{18\dot{\gamma}\, m_p}{St + 18\dot{\gamma}\,\Delta t} U_2^R = -F_2^\beta \tag{3.3}$$

The above expression for evaluating forces should be preferred over equation 3.2, since it provides for a more stable computation (though not necessarily a more accurate one). It hence avoids the possibility of choosing an overly conservative time step, and

we have hence implemented it for computing forces in the simulation model.

Since the wet layers are thin, the particles which interact via their wet layers will form a distinct 'liquid-bridge'. Thus a net attractive force due to the surface tension effects will also be experienced by the particles. In most practical situations, this force is weaker than the viscous forces (Ennis et al. (1991)). It is always directed along the centerline direction and its magnitude for the case of two equal sized particles can be estimated as:

$$F_c = \frac{\pi\, d_p\, \sigma}{1 + \tan(\frac{\phi}{2})} \tag{3.4}$$

where σ is the interfacial tension and ϕ is the wetting angle (Simons et al. (1996)). Since we have assumed the particles to maintain a constant wet layer thickness, we estimate ϕ by its maximum value of $\pi/2$. This assumption does not significantly influence the value of F_c since as seen from the expression, F_c is a relatively weak function ϕ. If a Capillary number, Ca, is defined as $Ca = \mu d_p \dot{\gamma}/\sigma$, the above expression can be rewritten as:

$$F_c = \frac{3\, m_p\, \dot{\gamma}^2\, d_p}{Ca\, St}. \tag{3.5}$$

The wet layers are assumed to merge whenever $R \leq (2h + d_p)$, where R is the distance between the centers of the two particles. No interactions due to the wet layers are considered whenever $R > (2h + d_p)$. In other words the liquid-bridge connecting the two particles is assumed to rupture exactly when $R = (2h + d_p)$. In a practical situation this point of rupture will not be sharp and will occur at a slightly higher value of R. The influence of these effects will be small in the limit $(h/d_p \ll 1)$, and are ignored in the present model.

The hard-core interactions between wet particles are modelled by the soft-particle overlap model rather than the hard-particle overlap one of chapter 2. We consider the soft-particle overlap model to be more appropriate for wet particles, since these

particles also remain under the influence of forces (viscous and capillary) which are more enduring in nature rather than impulsive. A 'stiffness' is hence imparted to particles by introducing a spring-type force which pushes them outwards when they overlap. This spring force is modelled as: $F_s = 0.5K(R - d_p)$, where K denotes the stiffness of the spring. The value of K should be chosen as the highest possible which still avoids an instability in computation. The choice of a still higher value can be achieved at the expense of lowering the time step. Dissipation during the hard-core interactions is modelled by introducing a dashpot which resists the centerline relative motion of approaching particles. The magnitude of this resistance is chosen high in order to model the high resistance predicted by the lubrication theory for nearly touching particles. This high resistance can be easily modelled by taking the limiting behavior of equation 3.3 as St approaches zero. This gives resisting forces of the type $F_2^\alpha = -(m_p/\Delta t)\, U_2^R = -F_2^\beta$. These forces are also equivalent to a zero coefficient of restitution type interaction since they in effect tend to damp the centerline relative velocity of approaching particles to zero by the end of time step.

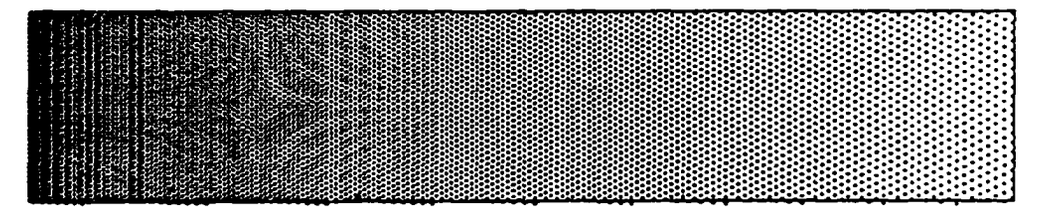

Figure 3.3: Particles in a two-dimensional plane with solid fraction linearly decreasing from 0.8 to 0.2 along the horizontal direction.

The above forces are introduced in the simulation model of shear flow of dry particles in chapter 2. These forces are made active (*i.e.* the wet layers are introduced) only after the time in simulation exceeds a parameter, t_{spray}, which represents the time of fluid spray over particles. At earlier times, no forces due to wet layers are

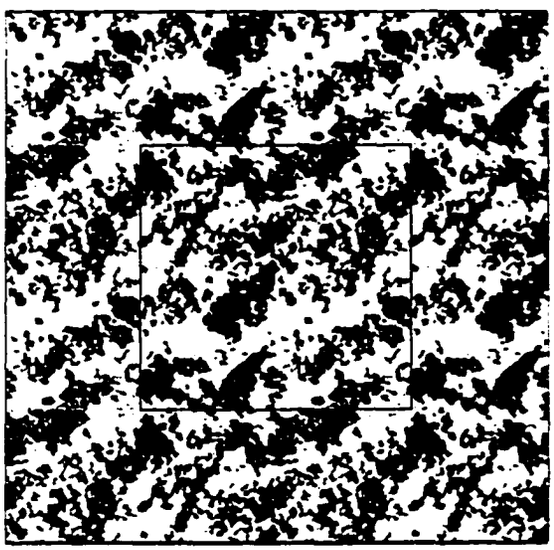

(a.) $St = 0.1$: $Ca = 1$

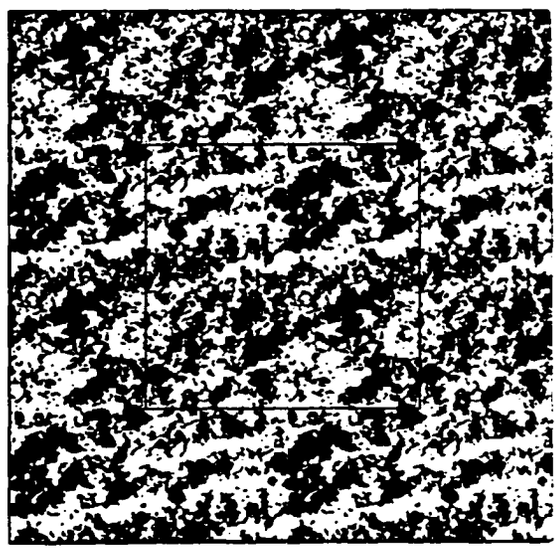

(b.) $St = 0.1$: $Ca = 10$

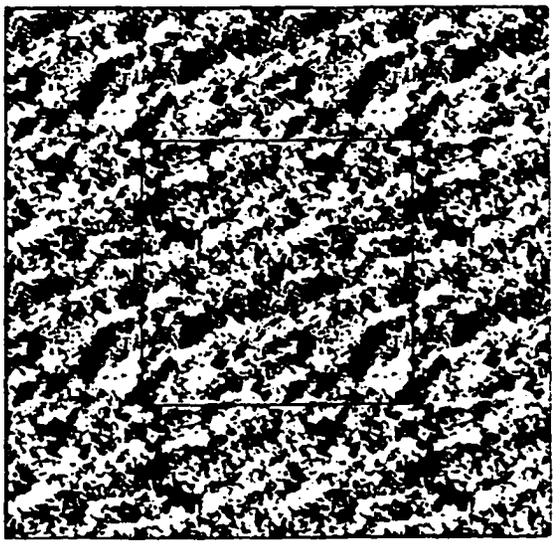

(c.) $St = 1$: $Ca = 1$

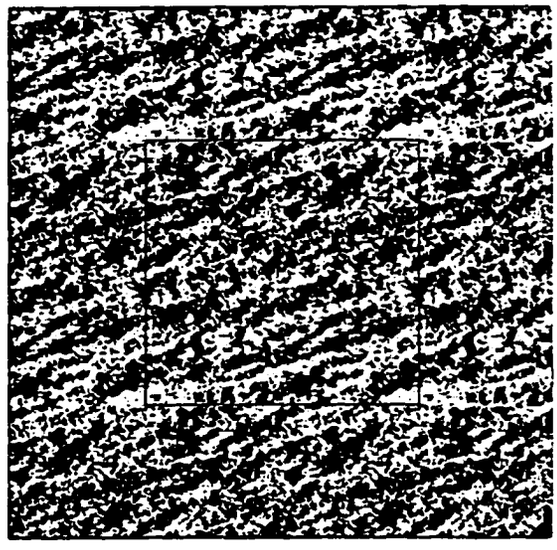

(d.) $St = 1$: $Ca = 10$

Figure 3.4: Snapshots of the simulation domain containing shearing wet particles incorporating the model of viscous interaction of section 3.1. The time is 100 dimensionless units while the time of the fluid spray is 25 dimensionless units.

considered, and the simulation is identical to the case when the particles are dry. This time of fluid spray, t_{spray}, is chosen such that the simulation with dry particles reaches steady state before the wet layers are introduced. A time of 25 dimensionless units was found to be a reasonable value for this purpose. The number of particles simulated were 40,000, the solid fraction was 0.4 (During the course of simulation, the solid fraction exhibits considerable local variation. This local value can be related from a figure to its quantitative equivalent with the help of Figure 3.3, which plots particles in a plane with a linear density variation along the horizontal direction.), the thickness of the wet layer was taken as 10% of the particle diameter, the dimensionless time step was taken as 0.01, while the value of dimensionless spring stiffness, defined as $K/\dot{\gamma}^2$, was chosen as 10. The choice of the time step and the spring stiffness maintained an average overlap between particles as less than 1% of the particle diameter. Though a finite overlap between particles violates continuity (conservation of mass) in the plane containing the particles, we noted previously in chapter 2 that this low value of overlap is a good approximation, and ensures a good accuracy of computation. The CPU time required by the simulation for these choice of parameters and 100 dimensionless time units was approximately 4 hours on a SGI Power Challenge workstation using a MIPS R10000 processor (better CPU times are reported here than in the corresponding problem of Chapter 2 due to some improvements in the program). The computation time scaled approximately linearly with the number of particles, the time step and the total simulated time.

After the particles are sprayed with the fluid at time $t = t_{spray}$, the simulation evolves towards a different steady state and results in particle agglomeration, the properties of the agglomerates being the function of parameters of the simulation such as the Capillary and the Stokes numbers. Figure 3.3 shows four results, with Stokes numbers of 0.1 and 1, and Capillary numbers of 1 and 10. Reaching steady state after the fluid spray takes approximately 50 more dimensionless time units. The snapshots in Figure 3.3 are taken at 100 dimensionless time units with the simulation running at steady state. It can be concluded from these figures that the tendency to-

wards agglomeration increases with the decreasing values of the Stokes and Capillary numbers. The figure provides some idea about the sensitivity of agglomerate size to order of magnitude changes in the value of the Stokes and Capillary numbers. It also provides an idea about the *relative* effects of changing the Stokes versus the Capillary numbers. One can conclude from this figure that changes in these two numbers which are approximately equal in magnitude have approximately the same magnitude of effect on agglomerate size.

A more rigorous analysis, correlating the agglomerate properties to parameters such as the Stokes and the Capillary numbers can be achieved if something equivalent of an image analysis can be performed over the pictures of the simulation domain. Several good software tools are available which could help in accomplishing this, and provide information about size, shape and density of the agglomerates in a given picture. Though in this work we have not attempted this, it seems that the quality of agglomeration in Figure 3.3 is not good enough for this purpose. As seen from this figure, the agglomerates lack a good definition and also carry a wide size distribution. There can be several possible reasons for this behavior. It can be due to the very nature of the process; as was discussed in chapter 1, particle agglomeration by granulation results in granules which are not very spherical and also carry a wide size distribution. The reason can also be that some assumptions in the simulation model distort the essential physics of the process. These assumptions could be the ignored lubrication effects, the ignored tangential forces and torques. It can also be due to some other ignored effect such as the cohesive forces between particles or non-Newtonian type flow behavior of the wetting layers.

The quality of agglomeration may also be compromised because our system is entirely homogeneous, since we have taken all particle and wetting layer properties to be identical. It is known from experimentation in granulation that large particles act as nucleation sites which grow by capturing the smaller ones. It is hence tempting to explore the effect of a distribution in properties such as the particles size and the wetting layer thickness. Unfortunately such an exercise is not quite straightfor-

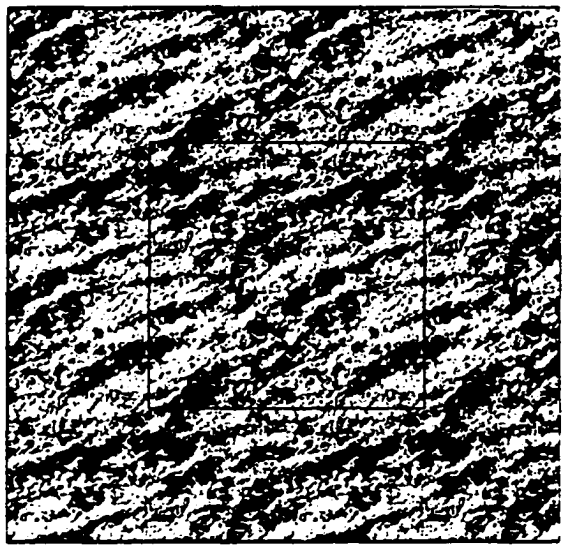

(a.) $St = 0.1$: $Ca = 1$

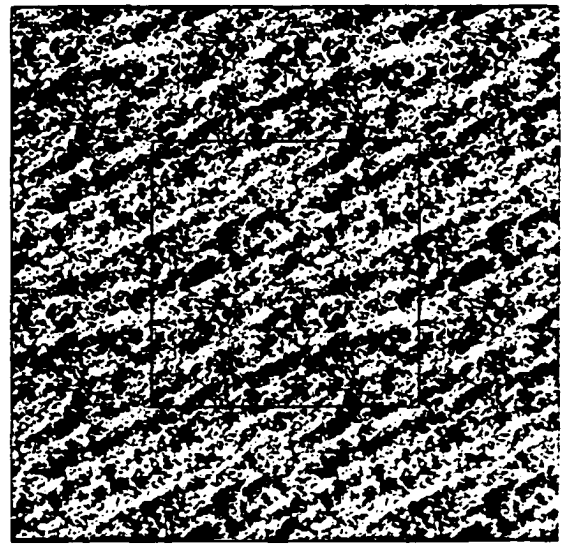

(b.) $St = 0.1$: $Ca = 10$

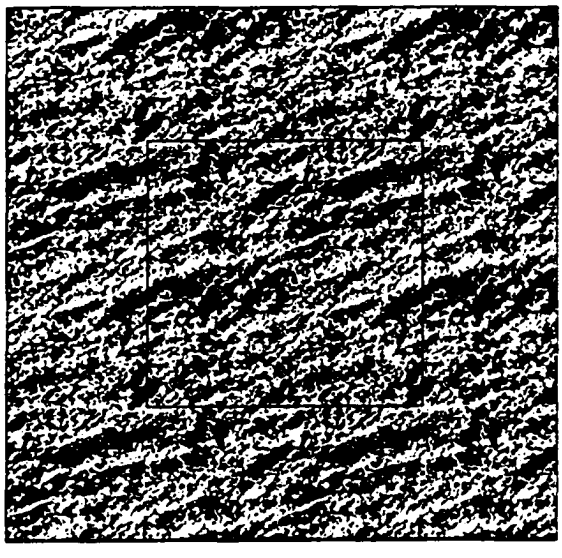

(c.) $St = 1$: $Ca = 1$

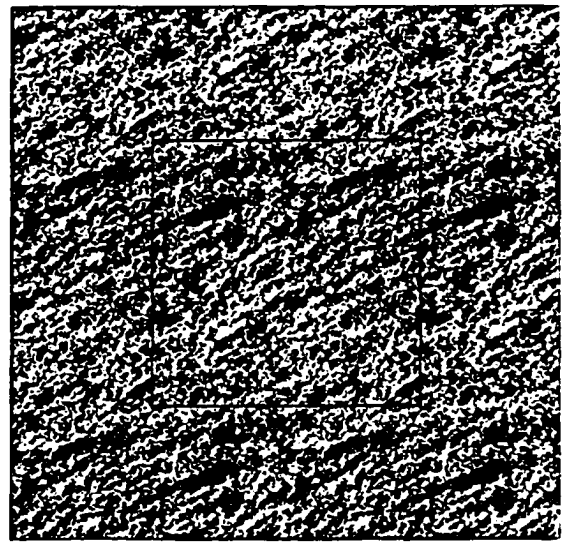

(d.) $St = 1$: $Ca = 10$

Figure 3.5: Snapshots of the simulation domain containing shearing particles. 20% of which are wet while the rest are dry. The model of viscous interaction is from section 3.1. The time is 200 dimensionless units while the time of the fluid spray is 25 dimensionless units.

ward, and we leave this as future work. We can however explore the effect of an inhomogeneity more easily in a somewhat artificial setting in which only a fraction of particles are made wet at the point of fluid spray and are maintained that way, while the rest are maintained dry. The model is somewhat artificial since the effects of liquid spreading are not considered. Wet particles are always assumed to remain wet while maintaining a constant wetting layer thickness, while the dry ones always remain dry. We still go ahead with the exercise since it may provide some insight on the effects of the introduction of an inhomogeneity. Figure 3.4 shows the steady state snapshots of the domain for the case when 20% of the particles are held wet. The choice of other parameters except for the total dimensionless time, which is now chosen as 200, remains the same as before. As seen from this figure the quality of agglomeration improves somewhat and one can detect agglomerates as clearer entities. The properties of agglomerates are correlated to the Capillary and the Stokes numbers in somewhat similar fashion as in Figure 3.3. It can hence be concluded from this figure that inhomogeneities in the system may assist in achieving agglomeration of good quality. In the next section we explore the effects of incorporating lubrication effects.

3.2 The model with centerline forces and lubrication effects

In this section we improve on the model developed in the previous section by incorporating lubrication effects in the centerline direction. Following the notation of the previous section, the lubrication forces experienced by two particles moving relative to one another in the centerline direction are given as (Kim and Karrila (1991)):

$$F_2^{\alpha} = -\mu(X_{11}^A - X_{12}^A)U_2^R = -F_2^{\beta} \tag{3.6}$$

where X_{11}^A and X_{12}^A are functions of the particle diameter and the dimensionless gap width. Though this relation is derived for the case when the particles are surrounded on all sides by infinite fluid, the expression will provide a good approximation for our case since the lubrication force predominantly arises from flow in the gap region along the centerline direction. The X_{11}^A and X_{12}^A functions are given in Kim and Karrila (1991) as:

$$X_{11}^A = 3\pi d_p \left(\frac{1}{4}\xi^{-1} + \frac{9}{40}\ln\xi^{-1} + 0.9954 + \frac{9}{336}\xi\ln\xi^{-1} + O(\xi)\right) \tag{3.7}$$

$$X_{12}^A = -3\pi d_p \left(\frac{1}{4}\xi^{-1} + \frac{9}{40}\ln\xi^{-1} + 0.3502 + \frac{9}{336}\xi\ln\xi^{-1} + O(\xi)\right). \tag{3.8}$$

Following previous section we will approximate U_2^R in equation 3.6 by its final velocity during a time step and rearrange this equation to yield the following expression for forces:

$$F_2^\alpha = -\frac{3\, m_p\, \dot{\gamma}\, \tilde{X}^A}{St + 3\,\dot{\gamma}\,\Delta t\, \tilde{X}^A}\, U_2^R = -F_2^\beta \tag{3.9}$$

where the function $\tilde{X}^A$ is defined as $\tilde{X}^A = 2(X_{11}^A - X_{11}^A)/(\pi\, d_p)$. As in the previous section we prefer this expression for force over equation 3.6 since it provides for a more stable computation, and have implemented it in the simulation model. The expression has the added advantage that while equation 3.6 carries a singularity at $\xi = 0$ (when particles touch), equation 3.9 does not. The above expression for forces is not valid when particles overlap (*i.e.* when $\xi < 0$), and for this case we model forces by the soft-particle collision model, as we did in the previous section.

Apart from the above nature of centerline viscous forces and the dimensionless time step, which is now chosen as 0.005, the rest of simulation model remains same as that in the previous section. Figure 3.5 shows the result for the case when all particles are wet and Figure 3.6 for the case when only 20% are held wet. The values

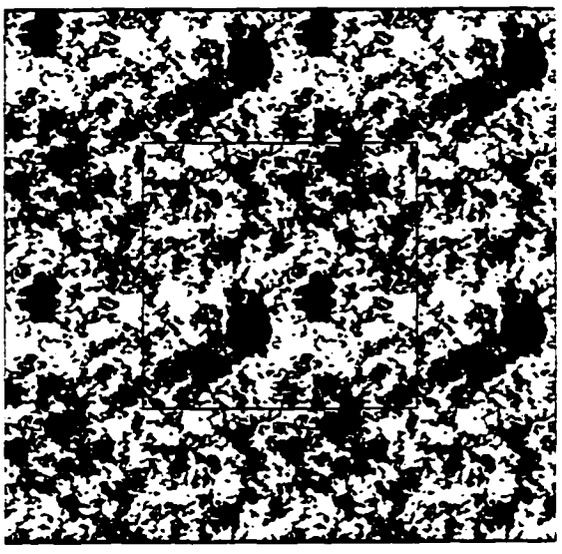

(a.) $St = 0.5$: $Ca = 1$

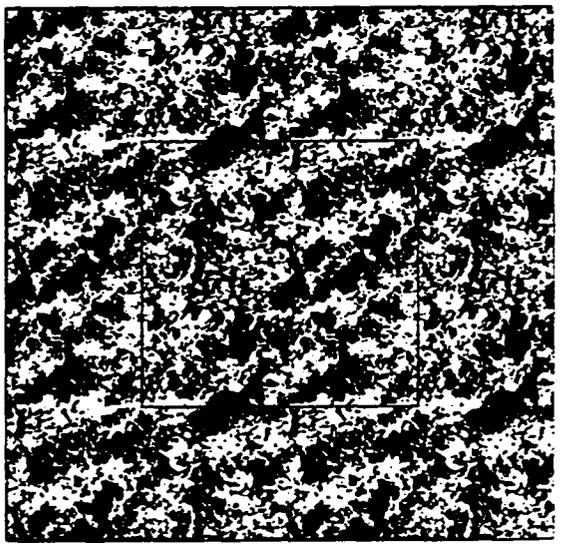

(b.) $St = 0.5$: $Ca = 10$

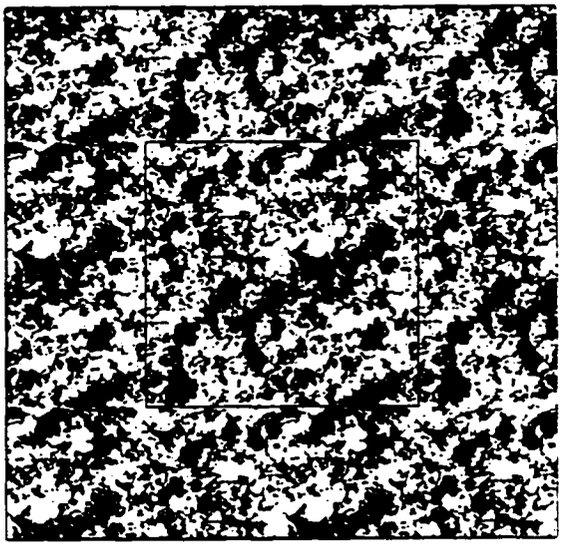

(c.) $St = 1$: $Ca = 1$

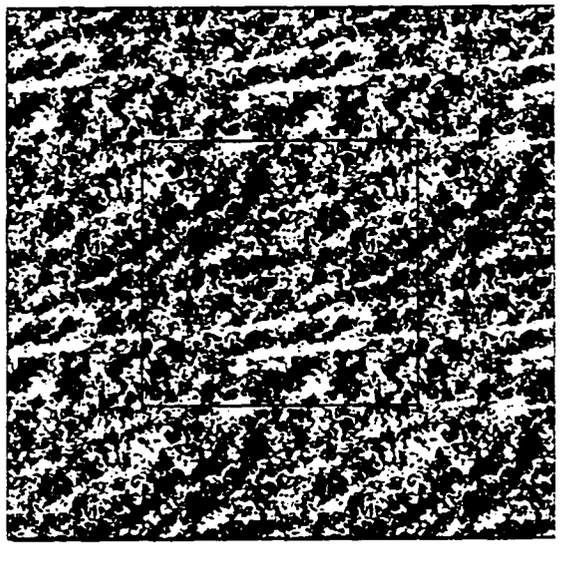

(d.) $St = 1$: $Ca = 10$

Figure 3.6: Snapshots of the simulation domain containing shearing wet particles incorporating the model of viscous interaction of section 3.2. The time is 100 dimensionless units while the time of the fluid spray is 25 dimensionless units.

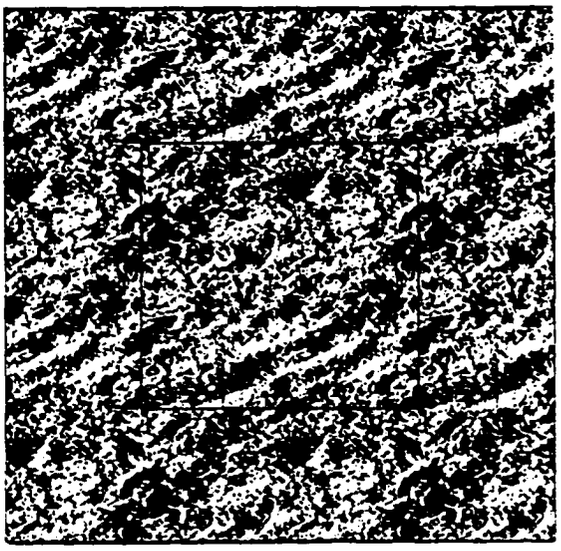

(a.) $St = 0.5$: $Ca = 1$

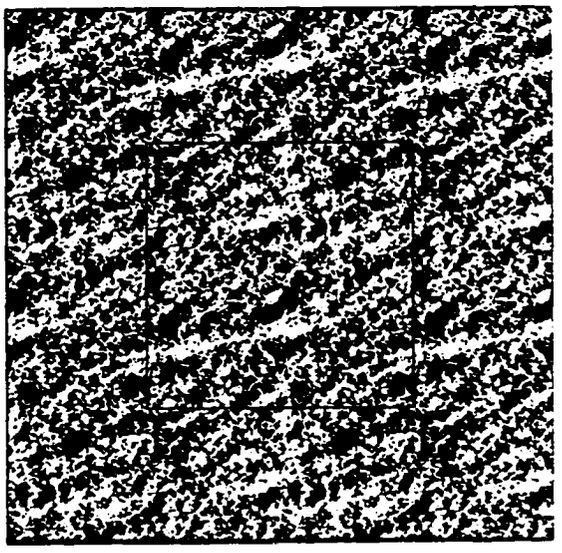

(b.) $St = 0.5$: $Ca = 10$

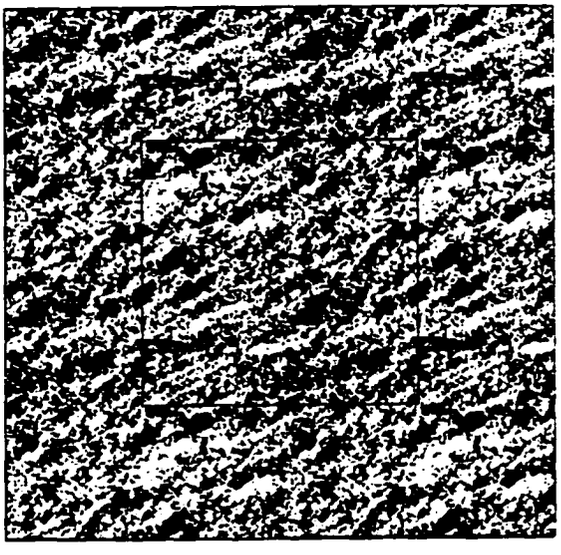

(c.) $St = 1$: $Ca = 1$

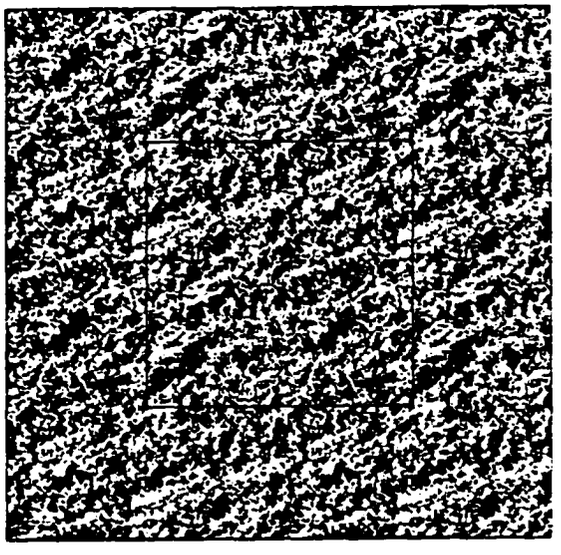

(d.) $St = 1$: $Ca = 10$

Figure 3.7: Snapshots of the simulation domain containing shearing particles. 20% of which are wet while the rest are dry. The model of viscous interaction is from section 3.2. The time is 200 dimensionless units while the time of the fluid spray is 25 dimensionless units.

of the Stokes number in these two figures were chosen as 0.5 and 1, while those of the Capillary number were chosen as 1 and 10. The two figures are more or less same in quality as Figures 3.3 and 3.4. This indicates that the incorporation of lubrication effects alone is not sufficient for achieving agglomeration of good quality.

3.3 Conclusions and future work

We were able to predict agglomeration by simulating shear flows of wet particles, and were also able to demonstrate sensible trends in agglomerate properties with respect to parameters such as the Stokes and Capillary numbers. Simulation results also allowed us to judge the relative sensitivity of agglomerate properties with respect to a change in these parameters. We also concluded from the simulation of a partially wet system that inhomogeneities in the system may contribute to good agglomeration. The drawbacks of the simulation model have been that the agglomerates carry a somewhat weak definition and also a large size distribution. We have argued that a possible reason for this behavior might be a failure to incorporate the essential physics of the process in the simulation model.

Future work should involve examining the assumptions of our model, identifying some ignored effects, and properly incorporating them in the model. The nature of the model and the set of input parameters that lead to good agglomeration should help one in identifying the important factors necessary for achieving good agglomeration. The simulation model can also be complemented nicely by experiments which are intended to closely represent the model. The fluidized-bed granular-flow Couette device of chapter 2, can assist in such an experimentation. We saw how this device can be used to make dry particles flow under conditions of approximately uniform shear. An idea to perform such an experiment for wet particles would be to use particles the surface of which can be made sticky by increasing the temperature of the fluidizing air (this phenomenon resembles sintering in high-temperature fluidized beds). A nice and controlled 'quenching' can then be achieved by a gradual reduction

of the shear rate and the temperature of the fluidizing air.

Further work along the developed lines looks promising. An improvement of and a systematic study with the simulation and experimental tools developed, can lead to a better understanding of the granulation process. To further this future development we present in the appendix a complete model which includes all viscous effects between particles interacting via their wet layers. Comparison of such simulations (unsuccessful so far) with experiments in the Couette device described above will be a great step forward.

Appendix

The complete model with lubrication effects

In this appendix we will extend the analysis of section 3.2 to incorporate the viscous forces in the tangential direction and also the torques over particles. So far we have not been able to successfully implement this analysis the simulation model. Its incorporation makes the computations unstable. Further work aimed at finding out the possible reasons for this behavior is left as a future exercise.

If $\mathbf{F}$ and $\mathbf{T}$ represent the generalized force and torque vectors with components being the components of forces (both centerline as well as tangential) and torques respectively on particles α and β, they can be related to the corresponding translational and angular velocity vectors, denoted by $\mathbf{U}$ and $\boldsymbol{\omega}$ respectively, as (Kim and Karrila (1991)):

$$\begin{bmatrix} \mathbf{F} \\ \mathbf{T} \end{bmatrix} = \mu \begin{bmatrix} \mathbf{A} & \tilde{\mathbf{B}} \\ \mathbf{B} & \mathbf{C} \end{bmatrix} \begin{bmatrix} \mathbf{U}^{\infty} - \mathbf{U} \\ \boldsymbol{\omega}^{\infty} - \boldsymbol{\omega} \end{bmatrix} \tag{A.1}$$

where $\mathbf{U}^{\infty}$ and $\boldsymbol{\omega}^{\infty}$ represent the translational and rotational components of the fluid velocity at infinity. The matrix with elements denoted as $\mathbf{A}$, $\mathbf{B}$, $\tilde{\mathbf{B}}$ and $\mathbf{C}$ is called the resistance matrix. Its elements ($\mathbf{A}$, $\mathbf{B}$, $\tilde{\mathbf{B}}$ and $\mathbf{C}$) are also matrices, the components of which are a function of the particle diameter and the gap width between the two particles. Rigorous definition of these elements and their exact dependence on the gap width can be obtained from Kim and Karrila (1991). The resistance matrix can be written in a simplified form for our two particle system if the coordinate system is chosen as the right handed 1-2-3 system of Figure 3.2. The above equation in a proper expanded form can then be written as:

$$\begin{bmatrix} F_1^\alpha \\ F_2^\alpha \\ F_1^\beta \\ F_2^\beta \\ T_3^\alpha \\ T_3^\beta \end{bmatrix} = \mu \begin{bmatrix} Y_{11}^A & 0 & Y_{12}^A & 0 & Y_{11}^B & -Y_{12}^B \\ 0 & X_{11}^A & 0 & X_{12}^A & 0 & 0 \\ Y_{12}^A & 0 & Y_{11}^A & 0 & Y_{12}^B & -Y_{11}^B \\ 0 & X_{12}^A & 0 & X_{11}^A & 0 & 0 \\ Y_{11}^B & 0 & Y_{12}^B & 0 & Y_{11}^C & Y_{12}^C \\ -Y_{12}^B & 0 & -Y_{11}^B & 0 & Y_{12}^C & Y_{11}^C \end{bmatrix} \begin{bmatrix} U_1^\infty - U_1^\alpha \\ U_2^\infty - U_2^\alpha \\ U_1^\infty - U_1^\beta \\ U_2^\infty - U_2^\beta \\ \omega_3^\infty - \omega_3^\alpha \\ \omega_3^\infty - \omega_3^\beta \end{bmatrix} \tag{A.2}$$

The subscripts on the elements of force and velocity vectors represent their components in the subscripted directions. The elements of the sub matrices **A**, **B**, **C** and **D**, under choice of the present coordinate system turn out to be either zero or their respective X and Y functions. The dependence of the X functions on the dimensionless gap width was provided in section 3.2, while those of the Y functions are given below:

$$Y_{11}^A = 3\pi d_p \left(\frac{1}{6}\ln\xi^{-1} + 0.9983\right) \tag{A.3}$$

$$Y_{12}^A = -3\pi d_p \left(\frac{1}{6}\ln\xi^{-1} + 0.2737\right) \tag{A.4}$$

$$Y_{11}^B = \pi d_p^2 \left(-\frac{1}{4}\ln\xi^{-1} + 0.2390 - \frac{1}{8}\xi\ln\xi^{-1} + O(\xi)\right) \tag{A.5}$$

$$Y_{12}^B = -\pi d_p^2 \left(-\frac{1}{4}\ln\xi^{-1} + 0.0017 - \frac{1}{8}\xi\ln\xi^{-1} + O(\xi)\right) \tag{A.6}$$

$$Y_{11}^C = \pi d_p^3 \left(\frac{1}{5}\ln\xi^{-1} + 0.7028 + \frac{47}{250}\xi\ln\xi^{-1} + O(\xi)\right) \tag{A.7}$$

$$Y_{12}^C = \pi d_p^3 \left(\frac{1}{20}\ln\xi^{-1} - 0.0274 + \frac{31}{250}\xi\ln\xi^{-1} + O(\xi)\right). \tag{A.8}$$

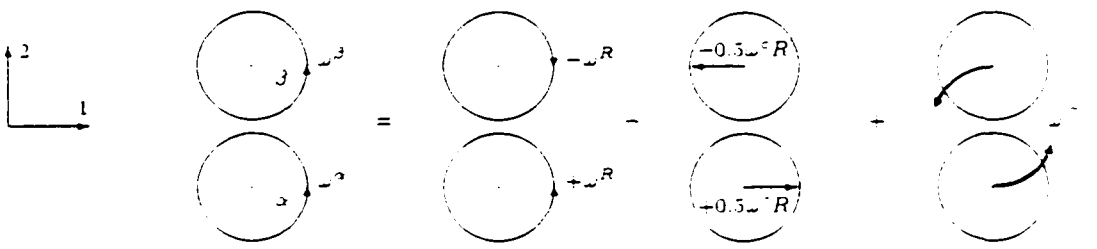

Figure A.1: Breakdown of an arbitrary rotational motion of two particles α and β past one another into purely relative and common rotational components.

The fluid velocities at infinity in equation A.2. can be taken as zero for our two particle system if we deal only with purely relative particle motions and do not consider the common translational and rotational components along the center of mass. We performed this exercise for the case of purely translational motion in section 3.1. In this section we are considering the rotations of individual particles as well. We will hence extend the analysis of section 3.1 by separating the common rotation along the center of mass as well. We follow a strategy similar to section 3.1 and define a relative rotational velocity as $\omega^R \equiv 0.5(\omega^{\alpha} - \omega^{\beta})$ and a common rotational velocity as $\omega^C \equiv 0.5(\omega^{\alpha} - \omega^{\beta})$. The rotational velocity of particle α is then $\omega^{\alpha} = \omega^C - \omega^R$, while that of particle β is $\omega^{\beta} = \omega^C - \omega^R$. Thus the two particles at any instant can be thought of as rotating about their centers with a common velocity of ω^C, and at the same time rotating with equal and opposite velocities of ω^R (particles α and β with velocities equal to $+\omega^R$ and $-\omega^R$ respectively). The rotation of particles along their respective centers with a common velocity of ω^C can be further broken down into their common rotation about the center of mass, and an equal and opposite translational motion along direction 1 with a velocity of magnitude $0.5\omega^C R$ (an example which considers a similar exercise is provided section 11.2.4 of Kim and Karrlia (1991)). The net result is represented in Figure A.1. Thus separating a common rotation along the center of mass will leave behind equal and opposite rotations about

the center of particles and equal and opposite translational motions along direction 1. Since the common rotation about the center of mass in Figure $A.1$ and a common translation in Figure 3.2 do not contribute to any force or torques, the velocity vector on the right hand side of equation $A.2$ can be written in a simplified form and the equation becomes:

$$\begin{bmatrix} F_1^\alpha \\ F_2^\alpha \\ F_1^\beta \\ F_2^\beta \\ T_3^\alpha \\ T_3^\beta \end{bmatrix} = -\mu \begin{bmatrix} Y_{11}^A & 0 & Y_{12}^A & 0 & Y_{11}^B & -Y_{12}^B \\ 0 & X_{11}^A & 0 & X_{12}^A & 0 & 0 \\ Y_{12}^A & 0 & Y_{11}^A & 0 & Y_{12}^B & -Y_{11}^B \\ 0 & X_{12}^A & 0 & X_{11}^A & 0 & 0 \\ Y_{11}^B & 0 & Y_{12}^B & 0 & Y_{11}^C & Y_{12}^C \\ -Y_{12}^B & 0 & -Y_{11}^B & 0 & Y_{12}^C & Y_{11}^C \end{bmatrix} \begin{bmatrix} +(U_1^R - 0.5\omega^C R) \\ +U_2^R \\ -(U_1^R - 0.5\omega^C R) \\ -U_2^R \\ +\omega^R \\ -\omega^R \end{bmatrix} \tag{A.9}$$

The above matrix equation allows one to evaluate the components of forces and torques from a knowledge of the translational and rotational velocity of particles. Following sections 3.1 and 3.2 we will attempt to re-evaluate the above expression for forces and torques by approximating the velocity vector on the right hand side by its final value during a time step. Proceeding along steps similar to those in sections 3.1 and 3.2 we obtain the following relations for forces in direction 1 and the torques:

$$F_1^\alpha = -\frac{\frac{m_p}{\Delta t}(U_1^R - 0.5\omega^C R)}{\frac{St}{3\dot{\gamma}\Delta t \tilde{Y}^A} - \frac{R\tilde{Y}^B}{kd_p\tilde{Y}^A} + 1} = -F_1^\beta \tag{A.10}$$

$$T_3^\alpha = -\frac{\frac{0.5m_p kd_p^2}{R\Delta t}(U_1^R - 0.5\omega^C R)}{\frac{k\,d_p\,St}{3\dot{\gamma}\Delta t R\tilde{Y}^B} + \frac{kd_p\tilde{Y}^A}{R\tilde{Y}^B} - 1} - \frac{\frac{0.25m_p kd_p^2}{\Delta t}\omega^R}{\frac{k\,St}{3\dot{\gamma}\Delta t\tilde{Y}^C} + 1} \tag{A.11}$$

$$T_3^\beta = -\frac{\frac{0.5m_p kd_p^2}{R\Delta t}(U_1^R - 0.5\omega^C R)}{\frac{k\,d_p\,St}{3\dot{\gamma}\Delta t R\tilde{Y}^B} + \frac{kd_p\tilde{Y}^A}{R\tilde{Y}^B} - 1} + \frac{\frac{0.25m_p kd_p^2}{\Delta t}\omega^R}{\frac{k\,St}{3\dot{\gamma}\Delta t\tilde{Y}^C} + 1} \tag{A.12}$$

where $\tilde{Y}^A = 2(Y_{11}^A - Y_{12}^A)/(\pi d_p)$, $\tilde{Y}^B = 4(Y_{11}^B - Y_{12}^B)/(\pi d_p^2)$, $\tilde{Y}^C = 8(Y_{11}^C - Y_{12}^C)/(\pi d_p^3)$ and k is defined as the square of the ratio of radius of gyration of a particle to

its radius. and is equal to 0.4 for spherical particles. The expression for centerline forces remain the same as in section 3.2. As was noted in sections 3.1 and 3.2. these relations (equations A.10, A.11, A.12 and 3.9) for evaluating forces and torques should be preferred over equation A.9 since they provide for a more stable computation. We added these forces and torques to the simulation of section 3.2. Unfortunately this made the computations unstable. The reasons for this behavior are not clearly understood at this point. Possible reasons could be an error in the above analysis or its incorrect implementation in the program. We leave a further investigation of this issue as future work.

Bibliography

AIDANPÄÄ, J.O., SHEN, H.H. & GUPTA, R.B. 1996. Experimental and numerical studies of shear layers in granular shear cell. *J. Eng. Mech. - ASCE* **122**(3), 187-196.

ADAMS, M.J., BRISCOE, B.J., KAMJAB, M. 1993. The deformation and flow of highly concentrated dispersions. *Adv. in Colloid and Interface Sci.* **44**, 143-182.

BOSSIS, G. & BRADY, J.F. 1984. Dynamic simulation of sheared suspensions. I. General method. *J. Chem. Phys.* **80**(10), 5141-5154.

BOUILLOT, J.L., CAMOIN, C., BELZONS, M., BLANC, R. & GUYON, E. 1982. Experiments on 2-D suspensions. *Adv. Colloid Interface Sci.* **17**, 299-305.

BRADY, J.F. & BOSSIS, G. 1988. Stokesian dynamics. *Ann. Rev. Fluid Mech.* **20**, 111-157.

BRADY, J.F. & BOSSIS, G. 1985. The rheology of concentrated suspensions of spheres in simple shear flow by numerical simulation. *J. Fluid Mech.* **155**, 105-129.

CAMPBELL, C. S. 1990. Rapid granular flows. *Ann. Rev. Fluid Mech.* **22**, 57-92.

CAMPBELL, C.S. 1989. The stress tensor for simple shear flows of a granular material. *J. Fluid Mech.* **203**, 449-473.

CAMPBELL, C.S. & BRENNEN, C.E. 1985. Computer simulation of granular shear flows. *J. Fluid Mech.* **151**, 167-188.

COMPO, P. 1989. Thermally induced agglomeration in fluidized beds. *Ph.D. Thesis* The City University of New York.

ENNIS, B.J., LI, J., TARDOS, G.I. & PFEFFER, R. 1990. The influence of viscosity on the strength of an axially strained pendular liquid bridge. *Chem. Eng. Sci.* **45**, 10, 3071-3088.

ENNIS, B.J., TARDOS, G. & PFEFFER, R. 1991. A microlevel based characterization of granulaton phenomena. *Powder Technology* **65**, 257-272.

HAPPEL, J. & BRENNER, H. 1973. In *Low Reynolds Number Hydrodynamics*. Nijhoff, Dordrecht.

HOGEKAMP, S., SCHUBERT. H. & WOLF S. 1996. Steam jet agglomeration of a water soluble material. *Powder Technology* **86**, 49-57.

HOPKINS, M.A. & LOUGE, M.Y. 1990. Inelastic microstructure in rapid granular flows of smooth disks. *Phys. Fluids A* **3**(1), 47-57.

HULBURT, H.M. & KATZ. S. 1964. Some problems in particle technology: A statistical mechanical formulation. *Chem. Eng. Science* **19**, 555-574.

ICHIKI, K. & HAYAKAWA, H. 1995. Dynamical simulation of fluidized beds: Hydrodynamically interacting granular particles. *Physical Review E* **52**(1), 658-670.

KHAN, M.I. & TARDOS, G.I. 1997. Stability of wet agglomerates in granular shear flows. *J. Fluid Mech.* **347**, 347-368.

KIM, S. & KARRILA, S.J. 1991. In *Microhydrodynamics: principles and selected applications.* Butterworth-Heinemann, Boston.

KOCH, D.L. 1990. Kinetic theory for a monodisperse gas-solid suspension. *Phys. Fluids A* **2**(10), 1711-1723.

KUNII, D. & LEVENSPIEL, O. 1991. In *Fluidization Engineering.* 2^{nd} Ed. Butterworth-Heinemann, Boston.

MACOSKO, C.W. (Editor) 1993. in Rheology: Principles, Measurements and Applications (Chapter 10). VCH Publishers, Inc., New York.

PIETSCH, W. 1996. Successfully use agglomeration for size enlargement. *Chem. Eng. Progress* **92**(4), 29-45.

RAMABHADRAN, T.E. 1975. On the general theory of solid granulation. *Chem. Eng. Sci.* **30**, 1027-1033.

SAVAGE, S.B. & SAYED, M. 1984. Stresses developed by dry cohesionless granular materials sheared in an annular shear cell. *J. Fluid Mech.* **142**, 391-430.

SCHAEFER, T. 1997. Melt agglomeration with polyethylene glycols in high shear mixers. *Ph.D Thesis*, The Royal Danish School of Pharmacy, Copenhagen, Denmark.

SIMONS, S.J.R. 1996. Modelling of agglomerating systems: from spheres to fractals. *Powder Technology* **87**, 29-41.

SIMONS, S.J.R., SEVILLE, J.P.K. & ADAMS, M.J. 1994. An analysis of the rupture energy of pendular liquid bridges. *Chem. Eng. Sci.* **49**(14), 2331-2339.

STONE, H. A. 1994. Dynamics of drop deformation and breakup in viscous fluids. *Ann. Rev. Fluid Mech.* **26**, 65-102.

TURIAN, R.M., HSU, F.L., AVRAMIDIS, K.S., SUNG, D.J., ALLENDORFER R.K. 1992. Settling and rheology of suspensions of narrow-sized coal particles. *AIChE Journal* **38**(7), 969-987.

WALTON, O.R. & BRAUN, R.L. 1986. Stress calculations for assemblies of inelastic spheres in uniform shear. *Acta Mechanica* **63**, 73-86.

WATANO, S., SATO, Y. & MIYANAMI, K. 1997. Application of a neural network to granulation scale-up. *Powder Technology* **90**, 153-159.

IMAGE EVALUATION
TEST TARGET (QA-3)

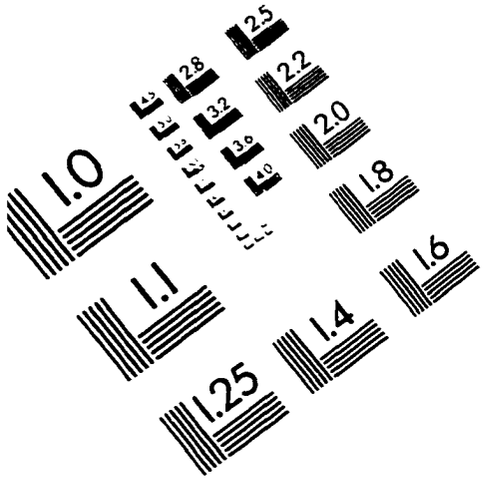

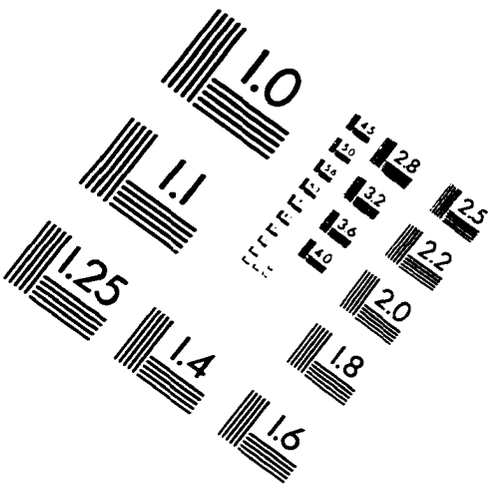

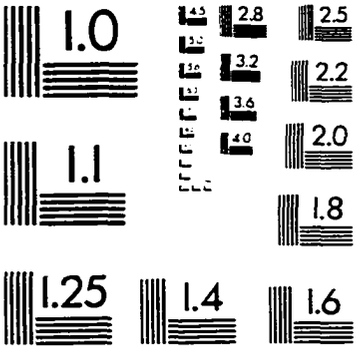

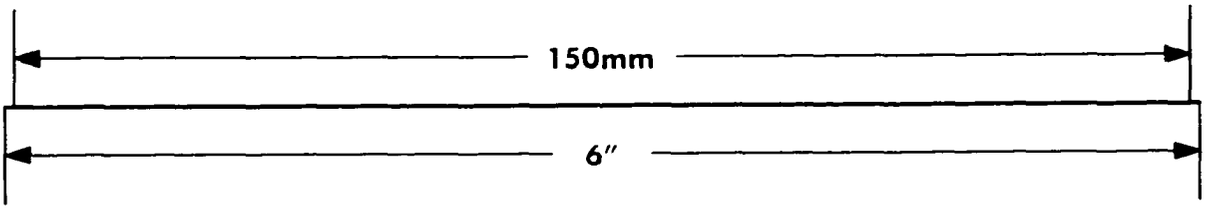

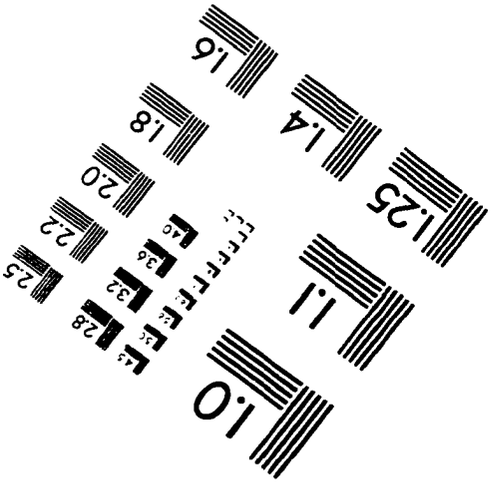

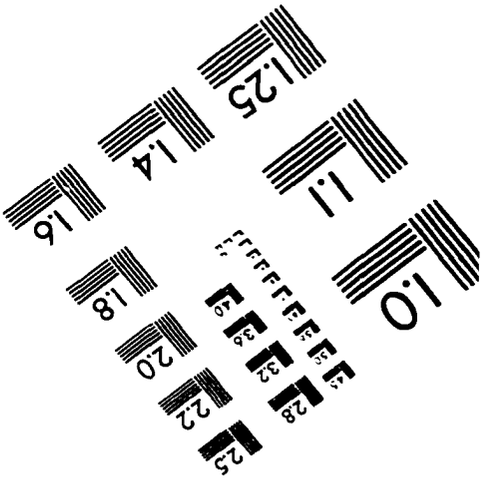

APPLIED IMAGE, Inc
1653 East Main Street
Rochester, NY 14609 USA
Phone: 716/482-0300
Fax: 716/288-5989